Carbon Nanotube–Based Electrochemical Detection of Endocrine Disruptors: A First-Principles Study of 17β-Estradiol Adsorption on (6,6) Single-Walled Carbon Nanotube

University of Turku
Department of Computing
Master of Science (Tech) Thesis
Biomedical Engineering and Health Technology
May 2026
Matilda Laurila

Supervisors:
MSc (Tech) Saara Sippola
Assoc. Prof. Emilia Peltola
Assoc. Prof. Milica Todorović
PhD Juho Heimonen

UNIVERSITY OF TURKU
Department of Computing

MATILDA LAURILA: Carbon Nanotube–Based Electrochemical Detection of Endocrine Disruptors: A First-Principles Study of 17β-Estradiol Adsorption on (6,6) Single-Walled Carbon Nanotube

Master of Science (Tech) Thesis, 84 p.
Biomedical Engineering and Health Technology
May 2026

Clean water is a fundamental requirement for life on Earth, but human activities have introduced a wide range of contaminants into aquatic environments. One particularly concerning group of pollutants is endocrine-disrupting chemicals (EDCs), which include natural hormones such as 17β-estradiol (E2). EDCs interfere with the normal function of the endocrine system in both humans and aquatic organisms, leading to adverse health effects. Because EDCs can exert biological effects at very low concentrations, their long-term impacts on human health are not yet fully understood. Currently, chromatographic methods represent the gold standard for monitoring these compounds in aquatic environment, but their high cost, complex instrumentation, and extensive sample preparation limit their suitability for real-time and in situ monitoring. Electrochemical sensors offer a low-cost and portable alternative. Beyond water quality monitoring, they also demonstrate significant potential for medical monitoring applications. Electrochemical sensors performance can be further enhanced by selecting appropriate electrode materials and strengthening the adsorption of target analytes on the electrode surface, thereby increasing the amount of analyte participating in the signal-generating electrochemical reactions.

In this thesis, the adsorption of E2 on a $(6, 6)$ single-walled carbon nanotube (SWCNT) was investigated computationally to gain an atomic-level understanding of the adsoprtion phenomenon. The objectives of the study were to identify stable and unique adsorption configurations of E2 on the $(6, 6)$ SWCNT surface and to determine whether the adsorption is governed by physical or chemical interactions. The study was conducted using density functional theory (DFT), integrated with the Bayesian Optimization Structure Search (BOSS) algorithm to efficiently explore the configurational space while reducing both computational cost and human bias.

Fourteen unique adsorption configurations were identified and classified into three structural groups based on geometric metrics. Analysis of the electronic structure revealed that E2 adsorption on the $(6, 6)$ SWCNT is governed by physisorption, dominated by van der Waals forces. These results clarify the adsorption mechanisms relevant to carbon nanotube–based electrochemical sensing. Overall, adsorption-based electrochemical sensors represent a promising and portable approach for the sensitive detection of EDCs in aquatic environments. By enabling more accurate and continuous monitoring, such sensing technologies could support preventive measures and facilitate compliance with environmental legislation, ultimately contributing to improved water quality.

Keywords: endocrine-disrupting chemicals, 17β-estradiol, single-walled carbon nanotubes, adsorption, density functional theory, bayesian optimization structure search, electrochemical sensors

TURUN YLIOPISTO
Tietotekniikan laitos

MATILDA LAURILA: Carbon Nanotube–Based Electrochemical Detection of Endocrine Disruptors: A First-Principles Study of 17β-Estradiol Adsorption on (6,6) Single-Walled Carbon Nanotube

Diplomityö, 84 s.
Lääketieteellinen tekniikka ja terveysteknologia
Toukokuu 2026

Puhdas vesi on elämän perusedellytys, mutta ihmisten toiminta on johtanut erilaisten epäpuhtauksien päätymiseen vesiekosysteemeihin. Huolestuttavaksi epäpuhtauksien ryhmäksi on noussut hormonitoimintaa häiritsevät yhdisteet (EDC-yhdisteet), joihin kuuluvat myös luonnolliset hormonit, kuten 17β-estradioli (E2). EDC-yhdisteet voivat häiritä sekä ihmisten että vesieliöiden hormonijärjestelmän toimintaa jo matalina pitoisuuksina, aiheuttaen haitallisia terveysvaikutuksia. Niiden pitkäaikaisia vaikutuksia ei myöskään vielä täysin tunneta. Kromatografiset menetelmät ovat EDC-yhdisteiden mittaamisen kultainen standardi vesiympäristöissä, mutta niiden korkea hinta, monimutkaisuus ja hitaus rajoittavat menetelmien soveltuvuutta reaaliaikaiseen ja in situ -seurantaan. Sähkökemialliset anturit ovat lupaava vaihtoehto alhaisen kustannustasonsa ja liikuteltavuutensa ansiosta. Vedenlaadun seurannan lisäksi niillä on potentiaalia myös lääketieteellisissä sovelluksissa. Anturien suorituskykyä voidaan parantaa sopivilla elektrodimateriaaleilla ja vahvistamalla kohdeanalyytin adsorptiota elektrodipinnalle. Tällöin suurempi määrä analyyttiä osallistuu signaalin tuottaviin sähkökemiallisiin reaktioihin.

Tässä työssä tutkittiin laskennallisesti E2:n adsorptiota $(6, 6)$-kiraaliselle yksiseinäiselle hiilinanoputkelle (SWCNT) atomitason ymmärryksen saavuttamiseksi. Tutkimuksen päätavoitteena oli tunnistaa vakaat ja uniikit E2:n adsorptiokonfiguraatiot SWCNT:n pinnalla sekä selvittää, perustuuko adsorptio fysikaalisiin vai kemiallisiin vuorovaikutuksiin. Tutkimus suoritettiin hyödyntämällä tiheysfunktionaaliteoriaa (DFT), joka yhdistettiin Bayesilaiseen optimointiin perustuvaan rakennehakualgoritmiin (Bayesian Optimization Structure Search, BOSS) konfiguraatioiden tehokkaaksi kartoittamiseksi. BOSS:n avulla vältettiin laskennallisten kustannusten kasvu sekä minimoitiin inhimillisiin valintoihin liittyvät virheet jättämällä ihminen suurelta osin prosessin ulkopuolelle algoritmin automaation ansiosta.

Tuloksena tunnistettiin neljätoista adsorptiokonfiguraatiota, jotka luokiteltiin kolmeen ryhmään rakenteen perusteella. Elektronirakenneanalyysi osoitti E2:n adsorboituvan $(6, 6)$ nanoputkelle fysikaalisten vuorovaikutusten, erityisesti dominoivien van der Waals -voimien, ansiosta. Tulokset edistävät atomitason ymmärrystä adsorptiomekanismeista, joilla on keskeinen rooli hiilinanoputkipohjaisessa sähkökemiallisessa yhdisteiden havaitsemisessa. Adsorptioon perustuvat sähkökemialliset anturit mahdollistavat lupaavan ja helposti siirrettävän ratkaisun EDC-yhdisteiden herkkään havaitsemiseen vesistöissä. Tarkempi ja ajallisesti kattavampi yhdisteiden seuranta anturiteknologialla mahdollistaa kokonaisvaltaisemman tilannekuvan saamisen vedenlaadusta, mikä parantaa edellytyksiä kohdennettuihin toimenpiteisiin sääntelyn avulla.

Asiasanat: hormonitoimintaa häiritsevät yhdisteet, 17β-estradioli, yksiseinäiset hiilinanoputket, adsorptio, tiheysfunktionaaliteoria, bayesilainen optimointirakennehaku, sähkökemialliset sensorit

Contents

List of acronyms

AES adsorption energy surface

ASE Atomic Simulation Environment

BO Bayesian optimization

BOSS Bayesian Optimization Structure Search

CNT carbon nanotube

COM center of mass

DFT Density functional theory

DOS density of states

E2 17β-estradiol

EDCs endocrine-disrupting chemicals

eLCB exploratory Lower Confidence Bound

GGA Generalized Gradient Approximation

GP Gaussian Process

HOMO highest occupied molecular orbital

LDA Local Density Approximation

LUMO lowest unoccupied molecular orbital

MBD many-body dispersion

MD molecular dynamics

PBE Perdew–Burke–Ernzerhof

pDOS partial density of states

PES potential energy surface

rbf radial basis function

RMSD root-mean-square deviation

SWCNT single-walled carbon nanotube

vdW van der Waals force

1 Introduction

Water is a fundamental prerequisite for life on Earth. From the earliest biology lessons in school, it is emphasized that life cannot exist without water. Although water covers most of the Earth's surface, only about 3% of it is freshwater, and only a small fraction of this is readily accessible for essential human uses, including drinking and sanitation. For this reason, concern over risks that affect the quality of these already limited water resources has increased globally over the past decades. Human activities have intensified climate change and pollution, highlighting the urgent need to improve water management, pollution prevention, and advanced treatment technologies to ensure the long-term sustainability of water environments [1].

Rapid development in various fields, such as packaging, pharmaceuticals, and plastic manufacturing, together with socioeconomic changes that have increased the use of new consumer goods, has led to the release of new types of compounds into aquatic systems. These compounds can contaminate water environments and cause negative effects on human and animal health upon exposure.

A particularly concerning group of pollutants are endocrine-disrupting chemicals (EDCs). These are chemicals that interfere with the normal function of the endocrine system and can cause adverse effects in both humans and wildlife. Substances such as natural and synthetic estrogens, bisphenol A (BPA), and phthalates are classified as EDCs. [2] Among natural estrogens, the female hormone 17β-estradiol (E2) is one of the most extensively studied due to its high biological potency. EDCs disrupt

hormonal signaling by mimicking natural hormones, blocking hormone receptors, or altering hormone synthesis, transport, and metabolism [3]. Because endocrine signaling is highly sensitive, even small disruptions can lead to significant biological consequences. Exposure to EDCs has been associated with fertility disorders, abnormal sexual development, early puberty, neurological and metabolic dysfunctions, and certain cancers. [2] Pregnant women, infants, and children are especially vulnerable during critical periods of development [3].

Exposure to EDCs is widespread in modern society due to their extensive use in various products, including pharmaceuticals, agricultural pesticides, consumer goods, and industrial processes. From there they are often unintentionally released into the environment during production, disposal, leakage, and through inadequate removal during wastewater treatment. Therefore they are frequently detected in environmental compartments such as soil, air, and water. [4] Human exposure to EDCs occurs through multiple pathways, including ingestion of food, pharmaceuticals, and drinking water, inhalation, and dermal contact. A major concern is that the effects of EDCs are often not immediately observable in humans or wildlife but may manifest only after long-term exposure, even at very low concentrations [2]. In animals, particularly aquatic species, exposure to EDCs originating from agricultural runoff and insufficient water treatment has been associated with developmental abnormalities, reproductive dysfunction, and population-level effects [5, 6].

This delayed impact highlights the need for early detection and effective prevention strategies. In response, regulatory authorities have begun to address EDCs through chemical and environmental legislation. For example, the European Union has introduced regulatory frameworks that require continuous monitoring of certain EDCs in aquatic environments and the establishment of exposure limits intended to prevent adverse effects [7]. However, the chemical diversity of EDCs and their occurrence at trace concentrations make reliable and accurate detection challenging,

emphasizing the need for improved analytical and sensing technologies to support regulation and environmental protection [2, 7].

Currently, chromatographic techniques, which are analytical methods used to separate, identify, and quantify chemical compounds in mixtures based on their physical and chemical properties, are considered the gold standard for monitoring EDCs due to their high accuracy, selectivity, and very low detection limits [7]. However, their practical application is limited by several factors, including high equipment costs, complex operation, and long analysis times [8].

One alternative approach to overcome these limitations is the use of electrochemical sensors, which are analytical devices that detect target compounds by measuring electrical signals generated during chemical reactions at sensor's surfaces. These kind of sensors have already been successfully applied in environmental and biomedical monitoring. They offer detection accuracy comparable to conventional analytical methods while also providing low-cost, simple, and sensitive platforms suitable for on-site and real-time measurements [4]. Importantly, sensor selectivity and performance toward target compounds can be enhanced through the adsorption of these compounds onto the sensor surface. Adsorption enables molecules to participate in electrochemical reactions, which generates the measurable signal. In addition, the choice of surface material determines device performance. Recently, carbon-based materials have emerged as promising sensor surface materials because aromatic compounds, such as all natural estrogens, are known to adsorb effectively onto them, making carbon nanotubes (CNTs), graphene, and their derivatives a promising surface materials due to their large surface area, high electrical conductivity, and stability under varying environmental conditions [4, 9, 10].

Although adsorption of aromatic compounds can be studied experimentally, even advanced techniques, such as atomic force microscopy, often struggle to provide sufficient resolution to accurately characterize interactions involving structurally

complex molecules, limiting detailed insight into sensor–compound interactions [11]. In addition, many experimental approaches used for development and optimization of electrochemical sensors rely heavily on trial-and-error procedures, which are not resource-efficient and, in the worst case, can result in significant time consumption and waste of tested surface materials and chemicals.

To address the limitations of experimental studies, investigations of the adsorption of aromatic compounds should be guided by a deeper understanding of atomic-level interactions, which can be achieved through computational simulations. However, computational studies face their own challenges, particularly the high computational cost that arises from extensive structural sampling required to identify stable minimum-energy molecular configurations, which correspond to the most physically realistic structures likely to occur in nature. As a result, some studies may rely on chemically intuitive initial configurations rather than performing an exhaustive search of the full configurational space, potentially missing relevant adsorption states. One effective strategy to reduce human bias and computational cost is the integration of machine-learning algorithms into the computational simulation pipeline. These approaches enable more efficient exploration of the energy surface and systematic identification of favorable adsorption configurations.

In this thesis, an adsorption structure search of E2 on a pristine $(6, 6)$ single-walled carbon nanotube (SWCNT) in vacuum was conducted. The study builds upon previous computational investigations of E2 adsorption on graphene, reported by Sippola [12]. This work follows a similar computational research framework, employing a workflow consistent with a previous study to extend the understanding of E2 adsorption from graphene to carbon nanotube systems, thereby providing a broader perspective on E2 adsorption across different carbon-based structures.

The computational part of this thesis was carried out using Bayesian Optimization Structure Search (BOSS) integrated with density functional theory (DFT).

BOSS employs an active-learning approach based on Bayesian optimization (BO), which allows efficient exploration of the adsorption energy surface (AES) without requiring exhaustive DFT calculations across the entire configurational space [13]. Instead, the method iteratively predicts and samples the most informative configurations, significantly reducing computational cost. The choice of E2 and the $(6, 6)$ SWCNT is motivated by experimental studies conducted by the Materials in Health Technology research group at the University of Turku, in which the same materials were employed.

However, no computational studies were found that specifically focus on E2 adsorption on pristine $(6, 6)$ SWCNT and therefore no direct comparison is currently available for the work presented in this thesis. Most of the available literature instead addresses other SWCNT chiralities or alternative carbon-based materials. For example, Zaib et al. conducted a computational investigation of E2 adsorption on (18,0) SWCNTs and graphene [10], while Sippola et al. studied E2 adsorption on graphene [14]. In addition, de Oliveira et al. focused on graphene oxide as the adsorption surface [15]. Despite differences in surface structure, these studies reported similar adsorption behavior, indicating that E2 adsorption on carbon-based materials is mainly governed by physical interactions and π–π stacking between the molecule and the surface.

In this context, the present work aims to bridge the existing research gap by systematically investigating E2 adsorption on pristine $(6, 6)$ SWCNTs using computational methods and by improving the understanding of molecular-level interactions between E2 and SWCNTs. In the future, studies of this kind can support the development of advanced electrochemical sensors for various applications, including environmental water-quality monitoring as well as biomedical uses such as fertility monitoring and dynamic tracking of hormone levels.

The research questions of this thesis are the following:

- RQ1: What does the existing literature indicate about the ability of carbon nanotube-based electrochemical sensors to detect 17β-estradiol (E2) in water samples?
- RQ2: What are the most stable and energetically favorable adsorption configurations of 17β-estradiol (E2) on a $(6, 6)$ single-walled carbon nanotube surface?
- RQ3: What types of interactions occur between E2 and a (6,6) single-walled carbon nanotube, and are any covalent bonds formed?

During the preparation of this thesis, AI-based tools were used as writing aids. Tools such as ChatGPT (version 5.2) and Google Gemini (Gemini 3) were employed to assist with grammar correction and wording refinement. The suggested corrections primarily addressed spelling, grammatical forms, prepositions, and punctuation.

The thesis begins with a detailed introduction to EDCs, along with currently available methods for their detection and monitoring in water. This is followed by a presentation of electrochemical sensing principles and adsorption phenomena, and concludes with a detailed discussion of CNTs as sensor surface materials. The computational methodology used in the simulation part of the thesis is then described. Subsequently, the methods and results of the computational study are presented. Finally, the thesis concludes with a discussion of the results, including their implications and limitations, and outlines future research directions related to the development of electrochemical sensors.

2 Technologies for water pollution detection

Water is a universal solvent, which makes it highly vulnerable to contamination from a wide range of substances. Water pollution refers to the presence of chemical, biological, or physical contaminants that alter the natural properties of water and make it unsafe for living organisms to consume. The origins of water pollution can be broadly classified as natural sources, such as volcanic eruptions and soil or sediment erosion, and sources resulting from human activities. Human-caused pollution arises from point sources, such as industrial and wastewater discharges, which release contaminants directly into water bodies and are generally regulated by authorities, as well as from non-point sources, such as agricultural runoff, which are harder to identify because pollution accumulates gradually over time. [16] Because water is essential for life, changes in its composition and quality can have widespread consequences for both humans and ecosystems. Even very small concentrations of certain pollutants can cause harmful and long-term effects, making water pollution a critical environmental and public-health concern.

The most concerning water pollutants are heavy metals, micro- and nanoplastics, and various synthetic organic compounds. Heavy metals are persistent and can bioaccumulate through the food chain, posing long-term risks to ecosystems and human health [17]. Micro- and nanoplastics can act as carriers for other pollutants

due to their large surface area and can facilitate their transport through aquatic systems. One particular concern is their ability to pass through biological membranes, accumulate in tissues such as the liver and blood vessels of aquatic organisms, and increase in concentration through food chains. [16] In addition, a growing range of pharmaceuticals, personal-care product chemicals, and other synthetic organic compounds has been detected in aquatic systems. Many of these substances exhibit endocrine-disrupting properties and can interfere with hormonal regulation in wildlife and humans even at low concentrations.

Reducing water pollution requires more than end-of-pipe solutions that focus only on treating pollutants after their release into the environment. It demands proactive prevention strategies supported by legislation, continuous monitoring, and sustainable industrial and agricultural practices. However, detection itself is often challenging: some pollutants occur at extremely low concentrations, exist in complex mixtures, or remain entirely unidentified. Without accurate and selective detection, developing effective purification technologies becomes nearly impossible, as the presence and distribution of harmful substances cannot be reliably determined. [18] Therefore, advancing both detection and purification technologies is essential to safeguard public health and ensure resilient ecosystems.

In this chapter, water pollutants classified as endocrine-disrupting chemicals and their impacts on both human health and wildlife are reviewed. Furthermore, current pollutant detection technologies are examined, their limitations are highlighted, and emerging advancements aimed at improving early detection are explored. These advancements enable more accurate environmental monitoring, support the development and enforcement of effective legislation, and ultimately contribute to more precise and efficient pollution removal strategies.

2.1 Endocrine-disrupting chemicals

Endocrine-disrupting chemicals (EDCs) are natural or synthetic substances that interfere with the normal functioning of hormonal systems. Commonly known examples of EDCs include compounds used in plastic products, such as bisphenol A (BPA), phthalates, and polychlorinated biphenyls, as well as natural hormones such as 17β-estradiol (E2). Although EDCs do not share a single structural pattern, many possess features such as aromatic rings, halogen atoms, or specific functional groups that allow them to mimic or otherwise interfere with natural hormones [2].

EDCs affect through endocrine system, which is a complex network of glands, hormones, and receptors providing the key communication channel and link between nervous system and vital body functions like reproduction, immunity, metabolism and behavior. Unlike the nervous system, which operates rapidly, endocrine signaling relies on slower biochemical communication and feedback loops. This makes hormonal balance highly sensitive to disruption, as even small disturbances may interfere with homeostasis. EDCs can mimic or block the action of endogenous hormones, most directly by binding to hormone receptors and activating or inhibiting them [3]. They may also disrupt endocrine signaling indirectly by altering hormone synthesis, degradation, transport proteins, or receptor expression [3]. While receptor binding resembles natural hormone action, the indirect mechanisms primarily disturb hormonal homeostasis.

Because endogenous hormones act at very low concentrations, even minimal exposure to EDCs can alter normal endocrine functions such as gene expression and cellular signaling. The extent of disruption depends on the binding affinity of the EDCs and the specific tissue they target. Notably, EDCs do not always follow the traditional toxicological principle of a dose-dependent response. Instead, many hormones and EDCs exhibit non-monotonic dose–response relationships, meaning that increasing the dose may produce different or even opposite biological effects. This

occurs because different concentrations can activate or inhibit hormone receptors in distinct ways, and multiple overlapping mechanisms, for example receptor binding, feedback regulation, and metabolic pathways, can dominate at different doses. [19] This poses significant challenges for risk assessment and regulation, as standard toxicology assumes that greater exposure leads to greater effect.

Sensitivity to EDCs also varies throughout the human life cycle. During critical developmental windows such as fetal growth, infancy, puberty, and menopause, hormone levels are naturally low or unbalanced. At these stages, even tiny exposures to EDCs can activate unbound receptors and induce biological responses that would not normally occur. [3, 20] For example, prenatal phthalate exposure has been shown to cause severe reproductive abnormalities in male rats, known as "phthalate syndrome" [5]. In addition to direct effects, exposure during sensitive periods may induce heritable epigenetic modifications, including changes in DNA methylation, histone modifications, or altered expression of non-coding RNAs, leading to long-term physiological consequences [20]. Prenatal exposure to polychlorinated biphenyls and BPA has been associated with altered DNA methylation and epigenetic regulation in genes involved in neurodevelopment, immune function, and brain-related processes [21, 22]. These findings raise significant concern regarding the potential cumulative and multigenerational risks posed by EDCs and highlight the importance of considering not only immediate toxicological effects but also long-term epigenetic consequences.

The importance of effective EDCs regulation is reflected in their substantial economic and health costs. As noted by Duh-Leong et al., EDCs-related diseases are estimated to cost approximately 340$ billion annually in the United States, while in the European Union the estimated burden is around 163€ billion per year [23]. These values demonstrate that insufficient regulation of EDCs has consequences not only for human health but also for economic sustainability. Nevertheless, regulation

of EDCs is currently complex and fragmented [2]. Due to their chemical structure diversity, broad range of sources, and the difficulty of establishing safe exposure limits resulting from their non-monotonic dose–response behavior, EDCs cannot be governed by a single regulatory framework and are instead addressed across multiple legislative domains and authorities, leading to regional differences in regulation between regions and countries [2]. For example, in the United States, the regulation of EDCs is shared between federal and state authorities. While the U.S. Environmental Protection Agency provides a national framework, individual states may introduce additional controls. Although this system allows flexibility and faster regional responses, it can lead to inconsistent protection levels and uneven risk management across regions [2].

At the international level, regulation of EDCs is guided primarily by the United Nations Environment Programme (UNEP) and the World Health Organization (WHO) through the International Programme on Chemical Safety (IPCS) [2]. This program coordinates risk assessments, develops common approaches to evaluating chemical safety, and responds to emerging environmental health issues. One outcome of the collaborations has been the European Commission's consensus statement on EDCs, which provided a scientific basis for defining EDCs and identifying priority areas for further research, such as developing more accurate, reliable, and selective detection methods, as well as improving our understanding of their mechanisms of action and long-term effects [2].

In the European Union (EU), EDCs are regulated through both chemical and environmental legislation. Chemical regulation is centralized under the Registration, Evaluation, Authorisation and Restriction of Chemicals (REACH) framework, overseen by the European Chemicals Agency. REACH applies broadly to chemical substances used in consumer and industrial products and places responsibility on manufacturers and importers to demonstrate their safety. Under this framework, the

EU has the authority to restrict or ban substances that pose unacceptable risks, and several EDCs, including BPA and certain phthalates, have already been restricted [2, 24].

In environmental context, the EU introduced the Water Framework Directive (WFD) in 2000 as the primary framework for water protection across Europe. The WFD aims to prevent the deterioration of water bodies and to achieve good ecological and chemical status in surface and groundwater systems [25]. In response to the increasing diversity of pollutants in aquatic environments, the directive was complemented by the Watch List mechanism [7]. The Watch List is a list of compounds that may pose environmental or health risks and for which additional data are required. It is revised every two years to add new substances and remove those for which sufficient data exist for further assessment. This mechanism supports targeted monitoring and the systematic collection of needed data on the compounds included in the list. The first Watch List was published in 2015 and included several steroidal estrogens, marking the beginning of broader EU-wide monitoring of these compounds [7].

In addition, the aquatic environment itself presents analytical challenges, as a single water sample may contain numerous different chemical compounds, of which only a few are regulatory interest. Detection and monitoring methods must therefore be highly selective toward the target substances in the presence of numerous interfering compounds. Moreover, improved monitoring techniques would enable regulatory authorities to better track EDCs in environmental pathways such as wastewater treatment effluents and agricultural runoff, thereby identifying critical sources and informing strategies to reduce the release of these compounds into aquatic systems.

2.1.1 Estrogens

Estrogens are a group of steroid hormones derived from cholesterol that exhibit estrogenic activity, such as regulating the ovulatory cycle, pregnancy and promoting the development of secondary sexual characteristics. Estrogens also have a role in the maintenance of bones, skin and central nervous system making a impact in humans overall health [26]. Estrogens are also classified as EDCs, because when released into the environment, they pose risks to ecosystems, aquatic organisms, and human health.

Estrogens primarily influence hormonal system functions by binding to intracellular estrogen receptors (ERα and ERβ), leading to modulation of gene expression and regulation of numerous physiological processes. Imbalanced estrogen levels can also be linked diseases like osteoporosis, breast cancer and cardiovascular diseases [27, 28]. Beyond their physiological roles, estrogens also serve important clinical purposes, as they are utilized in menopausal hormone therapy, hormonal contraception, and feminizing hormone therapy for transgender and gender-diverse individuals.

Estrogens can be categorized into two main subgroups based on their chemical structure: steroidal estrogens, which possess a steroid backbone with additional functional groups, and non-steroidal estrogens, which lack the steroid ring system [29]. They can also be classified based on their origin. Natural estrogens are compounds produced by humans and animals and are released into the environment mainly through excretion. The four naturally occurring estrogens in women are estrone (E1), 17β-estradiol (E2), estriol (E3), and estetrol (E4), each exhibiting distinct potency and physiological functions [30]. Their chemical structures are presented in the Figure 2.1. Of these, E1, E2 and E3 are the most biologically active and play dominant roles in endocrine regulation. This thesis focuses on 17β-estradiol, the most potent and biologically active natural estrogen. E2 has been included in the EU Watch List since 2015, highlighting its environmental relevance and toxico-

logical significance [7]. In addition, E1 is also included in the list [7]. Following this general overview of common estrogens, E2 is discussed in more detail in a dedicated section.

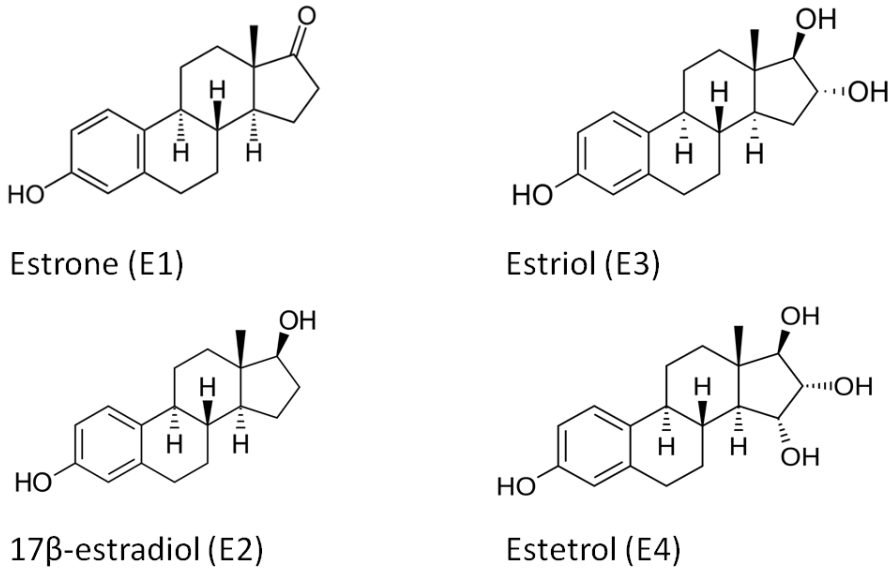

Figure 2.1: Chemical structures of the natural estrogens: estrone (E1), 17β-estradiol (E2), estriol (E3), and estetrol (E4).

Estrone $C_{18}H_{22}O_2$ is the oxidized form of E2 and represents weaker estrogenic activity, because its cyclopentane ring contains a carbonyl group instead of a hydroxyl group [29]. Therefore E1 serves as both a precursor and a metabolite of E2, with interconversion between the two forms catalyzed by 17β-hydroxysteroid dehydrogenase enzymes. E1 is primarily produced in the ovaries and, in premenopausal women, is the second most abundant circulating estrogen after E2. After menopause, E1 becomes the dominant circulating estrogen. [30] E1 is a major estrogenic compound in aquatic environments and commonly occurs as a degradation product of E2 [6]. According to the EU Watch List, the maximum accepted annual average concentration for E1 in surface water is 3.6 ng/L [7, 31].

Estriol $C_{18}H_{24}O_3$ is the weakest natural estrogen and contains three hydroxyl groups, making it more polar and less hydrophobic than E1 or E2. This increased

polarity contributes to its faster metabolism and lower persistence in biological and environmental systems [6]. E3 is mainly produced during pregnancy through fetal–placental metabolism, with the highest concentrations observed in the third trimester. It plays a role in ensuring sufficient oxygen and nutrient supply to the fetus by maintaining placental blood flow. Because E3 production reflects linked activity between the fetus and placenta, its measurement in maternal plasma or urine provides a valuable indicator of fetal condition during pregnancy. [30]

Estetrol $C_{18}H_{24}O_4$ is produced only during pregnancy by the fetal liver and placenta, but it has not been detected in other mammalian species, such as mice, rats, or rabbits, during pregnancy. Because of this unique characteristic, researchers have investigated whether E4 levels correlate with fetal well-being during pregnancy, but no such correlation has been found. [32] The four hydroxyl groups in the structure of E4 make it highly polar and less hydrophobic, resulting in high water solubility and low environmental persistence due to rapid aerobic biodegradation [33]. E4 is the only natural estrogen that exhibits tissue-selective estrogenic activity, meaning its effects depend on the specific receptors and its location in the body. It can act through activation (agonistic) or blocking (antagonistic) mechanisms. For example, it may exhibit neuroprotective effects in the brain while showing antagonistic activity in reproductive tissues by reducing follicle-stimulating hormone levels and thereby inhibiting ovulation, as well as in breast tissue by reducing the proliferation of breast cancer cells in the presence of E2. [32]

In addition to natural estrogens, environmental estrogens include synthetic chemicals, such as BPA and ethinylestradiol (EE2) (Figure 2.2), as well as naturally occurring plant-derived compounds. These compounds can also interfere with the normal function of hormonal systems in humans and wildlife. A major challenge is that many of these compounds do not share structural similarity with natural steroid hormones, making the prediction of their estrogenic activity difficult [28].

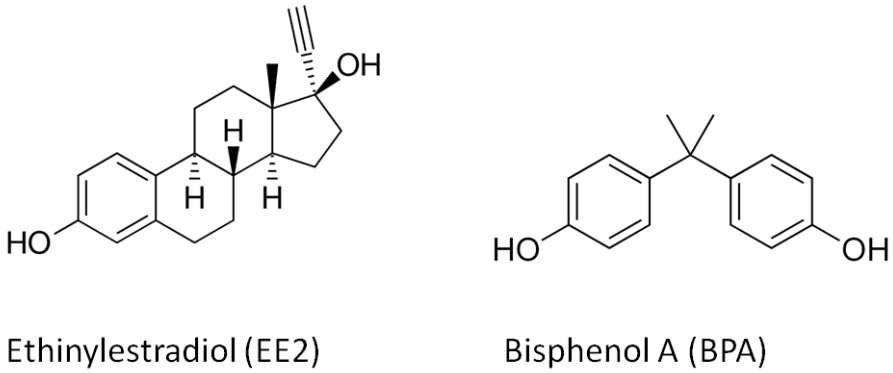

Figure 2.2: Examples of synthetic endocrine-disrupting chemicals: ethinylestradiol (EE2) and bisphenol A (BPA).

Synthetic estrogens are designed to mimic the biological activity of natural estrogens but with improved potency, stability, or biological availability, which is achieved by adding or modifying functional groups in the structure. They are widely used in clinical applications, including hormonal contraception, hormone replacement therapy, and cancer treatment in females, such as breast and ovarian cancers. The most commonly used synthetic estrogen in combined oral contraceptives is EE2 [32]. EE2 $C_{20}H_{24}O_2$ is a synthetic derivative of E2, which is why their structure is almost similar, as can be seen in the Figure 2.2. Only difference is the presence of an ethinyl group, which increases EE2 metabolic stability and persistence in both biological and environmental systems. Although EE2 is detected at lower concentrations than estradiol in aquatic environments, it exhibits strong estrogenic activity and has a maximum accepted annual average concentration of only 0.035 ng/L under the EU Watch List framework [7, 34]. Multiple studies have shown that chronic exposure to EE2 causes significant reproductive disruption in fish populations. Reported effects include feminization of male fish [35], disrupted oogenesis and gamete development in females [36], skewed sex ratios and reduced offspring production [35] and, in severe cases, population-level decline [36, 37].

2.1.2 17β-estradiol

E2 is synthesized enzymatically from cholesterol, primarily in the ovaries, but also in smaller amounts in the adrenal cortex, adipose tissue, hippocampus, and, in males, in the testes [30]. E2 is a key regulator of female reproductive physiology, which supports endometrial growth and maintains vaginal epithelium. Additionally, E2 plays an important role in neural plasticity and cognition, and its deficiency is linked to mood and cognitive disorders [38, 39]. E2 levels vary across life stages, as shown in Table 2.1. In premenopausal women, the menstrual cycle regulates E2 concentrations. E2 levels rise sharply prior to ovulation and remain elevated during the luteal phase.

Table 2.1: Typical concentrations of E2 in humans at different life stages [40].

Population group	**E2 Concentration (ng/L)**
Prepubertal children	< 20
Premenopausal women	30 – 800
Postmenopausal women	< 20
Pregnancy	up to 20 000
Men	< 40

The molecular formula of E2 is $C_{18}H_{24}O_2$. E2 has two cyclohexane rings, one aromatic phenol ring and a cyclopentane ring in its structure, as shown in Figure 2.3. Two hydroxyl groups are positioned such that one is attached to the aromatic ring and the other to the cyclopentane ring. Structurally, E2 differs from other estrogens in the number and spatial arrangement of its hydroxyl groups, which directly influences its binding affinity to estrogen receptors, making it the most potent estrogen [41]. Due to the rigid and nearly planar conformation of its steroid backbone, E2 can adopt an orientation that allows its aromatic ring to participate in π–π interactions with other aromatic compounds or carbon-based materials [42]. These interactions arise from attractive forces between the delocalized π-electron systems of aromatic rings.

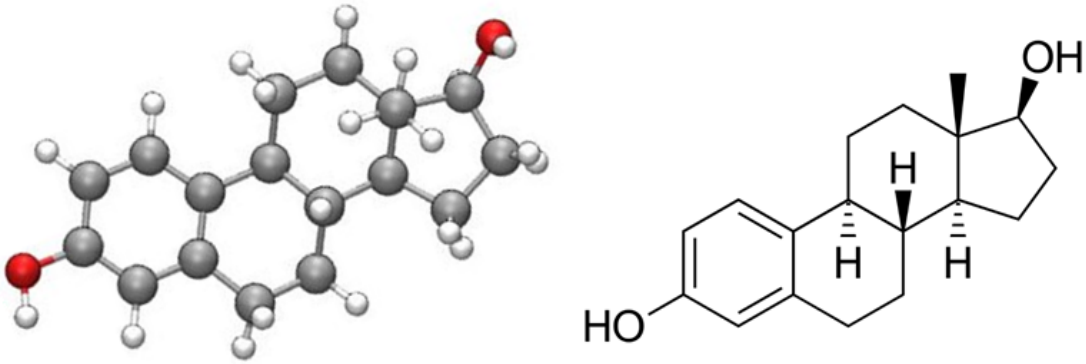

Figure 2.3: Molecular structure of E2 shown as a ball-and-stick model (left) and a skeletal formula (right).

E2 is widely used as a pharmaceutical compound, particularly in hormone replacement therapy and oral contraceptives, due to its potent estrogenic and antigonadotropic properties. At high concentrations, estradiol can inhibit ovulation and suppress the secretion of other sex hormones, making it a key component in many reproductive health medications [43, 44]. As a result of its widespread use, E2 enters the environment primarily through human and animal excretion and pharmaceutical waste [6].

The effects of E2 are not limited to humans. Even trace concentrations of E2 can cause significant endocrine disruption in wildlife. Under the EU Watch List, the maximum accepted annual average concentration for E2 is set at 0.4 ng/L [31]. Exposure to low ng/L concentrations of E2 has been shown to induce vitellogenin production, a biomarker of estrogenic exposure, in male fish [45, 46]. In aquatic organisms, such effects can lead to intersex development [35], disrupted reproductive cycles [6], and population-level declines [36]. Over time, these effects may propagate through the food web, raising concerns about indirect impacts on human endocrine health and ecosystem stability. These findings highlight the importance of sensitive and reliable methods for detecting E2 in aquatic environments.

2.2 Current methods for pollutant detection and monitoring

Current detection methods for EDCs rely heavily on chromatographic techniques, which remain the global gold standard for water pollutant analysis [31]. Chromatographic methods are based on the separation of compounds according to their different physicochemical properties, such as polarity, solubility, charge, and molecular size. These methods are also referenced in the EU Watch List framework as suitable approaches for achieving the required analytical performance [7].

In chromatography, separation occurs through the interaction of analytes between two phases: a stationary phase and a mobile phase. The analytes are dissolved in the mobile phase, which flows through or over the stationary phase. During this process, compounds in the mobile phase interact with the stationary phase with varying strengths. Stronger interactions with the stationary phase slow down the movement of the compounds, while weaker interactions allow them to migrate more rapidly, thereby enabling their separation and identification. [47] Depending on the nature of the mobile phase and the separation mechanism, chromatographic techniques can be classified into methods such as paper, liquid or gas chromatography.

For the detection of EDCs in water samples, chromatographic and chromatography–mass spectrometry methods are widely used due to their excellent accuracy, selectivity, and sensitivity [4, 7]. Mass spectrometry further enhances chromatographic methods by providing precise molecular identification after chromatographic separation based on ion mass-to-charge ratios and characteristic fragmentation patterns. Commonly applied techniques include gas chromatography–mass spectrometry, high-performance liquid chromatography, and liquid chromatography–mass spectrometry. A major advantage of these methods is their ability to identify multiple compounds in a single analytical run, which is particularly important given the

chemical diversity of EDCs in wastewater [8]. However, these methods also have several limitations. One major challenge is achieving sufficient detection accuracy to meet regulatory requirements. The EU Watch List framework requires Member States to continuously monitor substances included on the list and also defines how accurate monitoring tools and analytical methods must be to ensure reliable reported values [7, 25]. According to this framework, the limit of quantification (LOQ), which means the lowest concentration that can be measured accurately and reproducibly, should be approximately 0.1 ng/L, while the limit of detection (LOD), corresponding to the lowest reliably detectable concentration, should be around 0.03 ng/L [48]. It has been shown that these requirements present challenges even for many state-of-the-art and preferred analytical techniques, such as chromatographic methods, particularly when sample preparation and analytical conditions are not fully optimized, highlighting the growing need for more sensitive and robust detection strategies [8, 31].

Furthermore, chromatographic methods rely on expensive, large laboratory equipment that must be regularly maintained and operated by trained specialists. In addition, the optimization of analytical parameters, such as temperature and ion source settings, strongly influences the quality of the obtained results and requires specific technical expertise [8]. These techniques are also unsuitable for on-site or real-time monitoring because sample preparation is extensive and typically involves pre-concentration, extraction, and purification steps. Consequently, analysis must be carried out under controlled laboratory conditions, often resulting in long processing times [4].

Besides the chromatographic-based methods, also several other analytical strategies are used for the detection of EDCs. One important group consists of bioanalytical techniques designed to determine the biological activity of EDCs. These include cell- and enzyme-based assays such as cell proliferation tests and luciferase induc-

tion assays. In cell proliferation assays, estrogenic activity is evaluated by measuring changes in cell growth in hormone-responsive cells after the exposure to a sample that has target compounds [49]. Luciferase induction assays rely on genetically engineered cells in which activation of estrogen receptors triggers the expression of a luciferase gene, producing a measurable bioluminescent product that is proportional to the estrogenic activity of the sample and can be measured with luminometer [50]. While bioanalytical techniques offer valuable benefits, like providing information about the biological potency of compounds, they can be labor-intensive. Moreover, the identification and quantification of specific compounds require complementary chemical analysis. In addition, their use often requires cell culture, multiple handling steps, and long analysis times, which limits their practicality for routine or large-scale monitoring [4].

In addition to bioanalytical assays, several optical and immunochemical techniques have also been employed for the detection of EDCs. These methods include, for example, biofluorescence, enzyme-linked immunosorbent assays (ELISA), and surface-enhanced Raman scattering (SERS). Biofluorescence is based on detecting light emitted by fluorescent chemical compounds. In this approach, biological recognition elements are coupled with fluorescent markers such as dyes or labels. When these markers bind to the target compound, the fluorescence intensity changes. By measuring this change, the concentration of the target substance in the sample can be determined. [51] ELISA is method that relies on antibody–antigen interactions, typically performed using 96-well microplates. This method is user-friendly, compatible with a wide range of samples, and commercially available. However, one drawback is the high cost and labor-intensive production of specific antibodies for the method. [4] SERS is advanced spectroscopy-based technique that uses metal nanostructures to amplify the Raman scattering signal of molecules, enabling the detection and identification of extremely small quantities. SERS offers high sensitiv-

ity, narrow characteristic peaks, and strong photostability. Despite these advantages, SERS currently requires specialized laboratory facilities and cannot yet be widely applied for on-site analysis. [52]

As outlined above, the limitations of current detection methods have increased the demand for alternative approaches that are accurate, selective, efficient, and suitable for compact and on-site applications, while still providing analytical performance comparable to conventional laboratory-based techniques. These approaches must also address challenges arising from the nature of EDCs, including their chemical diversity and occurrence at very low concentrations. In this context, electrochemical sensing approaches have emerged as promising alternatives. These methods have already demonstrated high sensitivity in medical diagnostics, where analytes are present at extremely low concentrations, and offer advantages such as rapid response, portability, and low operational cost [53, 54]. As a result, electrochemical sensors represent a strong candidate for future environmental monitoring applications and are discussed in detail in the following section.

2.3 Electrochemical sensors for water purification

Electrochemical sensors are a subclass of chemical sensors, classified according to their operating principle. According to the International Union of Pure and Applied Chemistry (IUPAC), chemical sensors convert chemical information, like concentration or composition of an analyte, into an analytically meaningful signal. [55] In electrochemical sensors, this signal originates from changes in the electrochemical properties of the sensor's sensing surface.

An electrochemical sensor is built from two main components: a chemically sensitive surface, typically a semiconductive material, and a physicochemical transducer, (electrode), which produces the signal. The operating principle of electrochemical sensors is based on chemical reactions or interactions occurring at the surface of

the chemically sensitive material, leading to measurable changes in the electrical properties of the system. This pipeline is illustrated in Figure 2.4. Electrochemical sensors can be further categorized according to the type of electrical signal they measure [56].

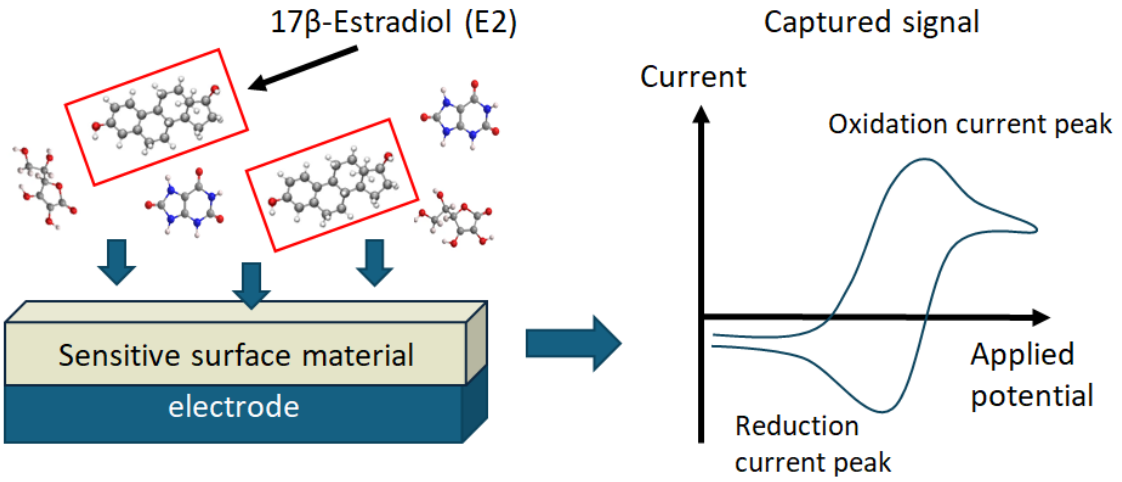

Figure 2.4: Schematic illustration of the working principle of an electrochemical sensor: interaction between the analyte and the electrode surface generates a measurable current signal. Figure adapted from [27], licensed under CC BY 4.0 (`https://creativecommons.org/licenses/by/4.0/`).

Electrochemical sensors offer several key advantages for environmental monitoring. They enable rapid screening of pollutants and are well suited for portable field deployment, allowing on-site assessment of water quality. In addition, they require only small sample volumes with minimal sample preparation, and their simple design makes them easy to use and resource-efficient.

There also exist electrochemical biosensors in which analyte recognition is based on specific biochemical interactions between a biological receptor that covers the electrode surface and the target analyte. Such receptors include antibodies, aptamers, and enzymes. In contrast, the non-biological electrochemical sensors that are within the scope of this thesis rely on physicochemical interactions between the analyte and the electrode surface. Because these sensors do not require biologi-

cal components, they typically exhibit greater stability, durability, and tolerance to environmental variations, such as temperature and pH changes. Another key advantage is their rapid response time, since signal generation does not depend on binding kinetics, which is often the case in electrochemical biosensors.

Different electrochemical sensors have already been tested for detecting E2 in water samples. For example, Moraes et al. [57] developed an electrode based on reduced graphene oxide combined with a metal–porphyrin complex, which enhanced the electrochemical response and improved the selectivity toward E2. The modified sensor demonstrated clear selective discrimination between E2, carbendazim, and carbaryl, and produced a well-defined irreversible oxidation peak for E2 at approximately $+0.54V$ due to the electrochemical reaction occurring at the sensor surface. The monitored peak represents the electrochemical signal indicating the presence of E2. The peak intensity reflects the sensor sensitivity, while its position indicates selectivity against interfering compounds. The observed detection limit for this electrode system was 1.4 ng/L, which is typical E2 concentrations reported in natural surface waters in Europe (approximately $0.1 - 10$ ng/L) [58]. In another study, similar electrochemical behavior was observed. Silva and Pereira [59] evaluated a sensor modified with a molecular imprinted polymer as the sensing material for the selective detection of E2 in environmental water samples. Their results showed that all tested electrode configurations produced an oxidation peak at approximately $+0.60V$. This peak corresponded to the irreversible oxidation of the hydroxyl group located on the aromatic ring of the E2 molecule, confirming the same electrochemical oxidation mechanism reported in Moraes et al. study [57].

The performance of an electrochemical sensor depends largely on several key factors, including electrode material properties, analyte–surface interactions, and operating conditions. Many of these factors can be directly influenced by the choice of chemically sensitive material on the electrode surface. By optimizing the sur-

face material, the sensor can be improved to be more selective toward a specific compound. This can be achieved through surface functionalization with tailored chemical groups or by developing and testing new materials with enhanced affinity and electrical conductivity. Improved sensitive materials strengthen interactions between the target molecule and the electrode surface, for example through adsorption phenomena, increasing the number of molecules participating in oxidation or reduction reactions and thereby improving the detection signal. In the case of E2, available evidence suggests that adsorption is a prerequisite for its electrochemical oxidation and subsequent detection [60]. In addition, increased selectivity enables reliable sensor operation in complex environments, such as aquatic systems, where many chemically similar compounds may be present. A selective sensor response minimizes interference from these compounds and ensures accurate measurements.

Carbon nanotubes (CNTs) have gained considerable attention as electrode materials due to their unique electrical, chemical, and structural properties, which can enhance sensitivity toward target compounds [61, 62]. Compared with commonly used electrode modifiers such as silver or gold nanoparticles, CNTs are less expensive, more chemically stable, and widely available, making them an attractive option for scalable sensor development.

2.3.1 Adsorption of organic compounds onto carbon-based materials

Adsorption is a phenomenon where atoms, ions, or molecules adhere to a surface from a gas, liquid, or dissolved solid phase. According to the IUPAC, adsorption is defined as "an increase in the concentration of a dissolved substance at the interface of a condensed and a liquid phase due to the operation of surface forces. Adsorption can also occur at the interface between a condensed and a gaseous phase" [63]. In general, adsorption occurs at the surface of materials when molecules transfer from

a gas or liquid phase onto a solid surface, forming a thin interfacial layer. This layer of substances can interact with the surface through physical forces, such as van der Waals (vdW) interactions (physisorption), or through chemical bonding, such as the formation of covalent or hydrogen bonds (chemisorption). During the adsorption process, the adsorbed substances form a thin film on the surface. The surface is referred to as the adsorbent, and the substance that adheres to the surface is called the adsorbate.

Adsorption can be used to improve the detection efficiency of certain analytes in electrochemical sensors. Through adsorption, a greater number of target molecules accumulate at the electrode surface, increasing the local analyte concentration and thereby enhancing their availability for electrochemical reactions such as oxidation and reduction. In some cases, such as for E2, successful adsorption is a prerequisite for electrochemical characterization, as interactions with carbon-based materials have been shown to be adsorption-controlled. Although E2 adsorption does not directly generate an electrochemical signal, it creates favorable conditions for oxidation–reduction reactions, thereby enhancing signal intensity and detection sensitivity [60].

Physisorption and chemisorption differ in their interaction mechanisms and energetics. Physisorption is the weaker form of adsorption, governed by physical forces such as vdW interactions, dipole–dipole interactions, and dispersion forces [64]. The most common physisorption forces arise from sudden fluctuations in electron density that create temporary dipoles, also known as vdW interactions. Because these forces are relatively weak, adsorbate molecules are loosely positioned on the surface, typically at a distance of about 3–5 Å from the surface. Under favorable conditions, such as high temperatures, these weak interactions can lead to the formation of multiple molecular layers on the surface. Physisorption is non-specific and can occur between almost any gas–solid combination under suitable conditions. Because

the intermolecular forces involved in the process are weak, small changes in external parameters can easily disturb the adsorption equilibrium, resulting in rapid desorption. [65] Therefore, physisorption is characterized by low adsorption energies and high reversibility.

On the other hand, chemisorption occurs when chemical bonds, such as carbon–carbon or metal–oxygen bonds, form between the adsorbate and the surface [64]. Chemisorption favors low temperatures and high pressure conditions. Compared to physisorption, chemisorption is more specific because it depends on the chemical nature of the surface and the functional groups of the adsorbate. Chemisorption is typically limited to a single molecular layer on the surface due to the nature of chemical bonding. Additional layers cannot form through chemical bonding once the available surface sites are occupied by the first layer of adsorbates. The distance between the adsorbate and the adsorbent is typically about 1–2 Å, which is characteristic of covalent bonds. [65] Because covalent bonding governs chemisorption, breaking these interactions requires significant energy. Consequently, desorption is often slow or irreversible under standard conditions. In practical applications, strong chemisorption can sometimes be disadvantageous. For instance, in electrochemical sensors, excessively strong adsorption of reaction products or biomolecules may lead to surface fouling, thereby reducing sensor sensitivity and long-term performance [66].

Studies have shown that the main governing forces in E2 adsorption on carbon-based materials are physical interactions [67, 68]. Because E2 contains an aromatic ring, it can interact with the aromatic carbon structures of materials such as CNTs and graphene through π–π stacking [9, 10, 14]. This interaction improves the stabilization of the molecule on the surface prior to oxidation. Adsorption based on physical forces can be advantageous in sensing applications where reversible interactions between the target compound and the surface are preferred over strong, irreversible binding.

2.3.2 Single-walled carbon nanotubes as electrode materials

As discussed earlier, sensor performance can be significantly improved by careful selection of the electrode's surface material. Various types of carbon-based nanomaterials have attracted considerable attention due to their unique properties, as well as the wide availability of carbon compared to many rare or precious metals. In this thesis, particular focus is placed on single-walled carbon nanotubes (SWCNTs), as they are employed in the computational part of the thesis.

The CNTs were first described in the early 1990s. Since then, CNTs have attracted significant research interest across various fields due to their remarkable and unique physicochemical properties. CNTs are tubular nanostructures that belong to the family of carbon allotropes. In their structure, sp^2-hybridized carbon atoms are arranged in a hexagonal, honeycomb-like lattice forming a graphene sheet that is rolled into a seamless cylindrical tube. [69] CNTs can be classified into two distinct groups based on the number of concentric layers of carbon atoms. Single-walled carbon nanotubes SWCNTs consist of a single cylindrical layer of carbon atoms, whereas multi-walled carbon nanotubes (MWCNTs) comprise several concentric layers leading to enhanced mechanical strength but also increased structural complexity. In this thesis, particular focus is placed on SWCNTs, as they are employed in the computational part of the thesis

CNTs also vary in their electronic properties and diameter, which depend on their chirality, described by the chiral vector (n, m) as presented in the Figure 2.5. This vector defines how the graphene sheet is rolled to form the cylindrical structure. Based on the chiral vector, CNTs can be categorized into three main types. Armchair CNTs, characterized by the chiral vector ($n = m$), exhibit metallic behavior and a highly symmetric periodic structure. Zigzag CNTs, defined by ($m = 0$), can display either metallic or semiconducting behavior depending on their structural parameters. Chiral CNTs, with ($n \neq m$ and $m \neq 0$), generally possess semiconducting properties. [69]

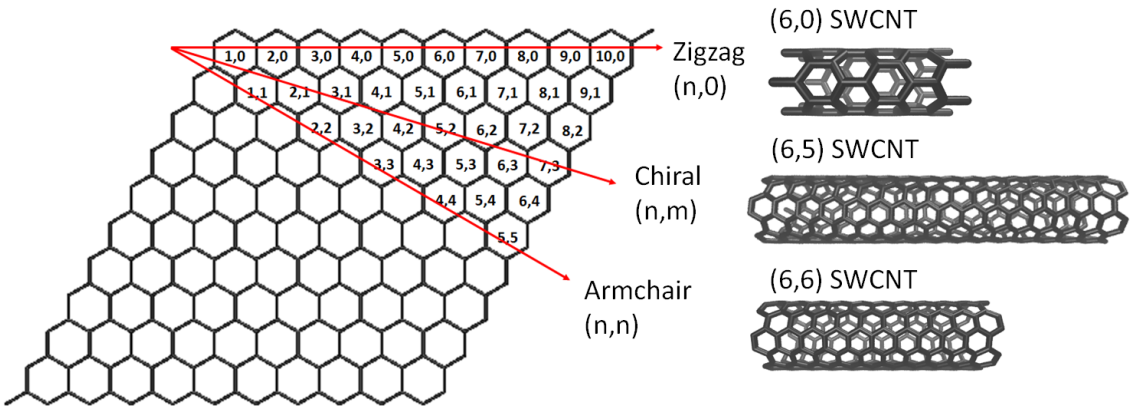

Figure 2.5: Chiral vector of a carbon nanotube and examples of different types defined by chirality: zigzag $(n, 0)$, chiral (n, m), and armchair (n, n).

The diameter of CNTs is typically only a few nanometers, while their length can extend to several tens of micrometers. This geometry results in an extremely high surface-area-to-volume ratio, making CNTs excellent materials for applications that require extensive contact surfaces, such as catalysis and sensing. CNTs also exhibit a wide range of remarkable physical properties arising from their hollow structure and unique arrangements of electrons, including low density, high electrical and thermal conductivity, high tensile strength, and high thermal and chemical stability [69].

Table 2.2 summarizes the structural properties of three different chirality types of SWCNTs, based on values reported in computational studies [70, 71, 72]. The unit cell length reported in the table refers to the smallest repeating structural unit along the SWCNT long axis. Because chiral SWCNT, such as the (6,5) SWCNT, have a helical atomic structure along the tube axis, their unit cell lengths are much longer than those of armchair or zigzag types. The unit cell length can influence the SWCNT's electronic properties and surface reactivity, which in turn can affect electron transfer and analyte adsorption.

In the field of environmental technology, CNTs have been employed for pollution detection in air and water matrices, as well as for pollutant removal in water through adsorption processes integrated with electrochemical techniques [61, 73, 74].

Table 2.2: Structural properties of SWCNTs with different chiralities [70, 71, 72].

Chirality (n, m)	Chirality type	Electronic type	Diameter (Å)	C–C bond length (Å)	Unit cell length (Å)
(6,6)	Armchair	Metallic	8.2	1.42	2.46
(6,5)	Chiral	Semiconducting	7.47	1.43	40.75
(6,0)	Zigzag	Metallic	4.83	1.43	4.30

This results from the ability of CNTs to become either hydrophilic or hydrophobic through functionalization and their strong adsorption capacity, including π–π stacking interactions with aromatic compounds [61, 73, 75]. In such applications, CNTs selectivity and sensitivity are typically improved by introducing functional groups onto the pristine CNT structure or by immobilizing biological recognition elements, such as enzymes or aptamers, to create CNT-based biosensors [61]. Beyond environmental applications, CNTs have also been extensively studied in the biomedical field for example as carriers for drugs and genes in cancer treatment, as well as in diagnostic tools such as antibody detection platforms [76].

Both experimental and computational studies have identified that adsorption between SWCNTs and EDCs, such as bisphenol A, EE2, and E2, is dominated by π–π stacking and hydrophobic interactions between the aromatic structures of the pollutants and the SWCNT surface [9, 10]. These interactions originate from the hexagonal carbon lattice and delocalized π-electron system of SWCNTs, which facilitate strong noncovalent binding with aromatic adsorbates. However, adsorption behavior on SWCNT surfaces is not uniform across all chiralities, as it depends on both electronic structure and surface geometry. For example, Seo et al. demonstrated that dopamine adsorption differs significantly between $(6, 5)$ and $(6, 6)$ SWCNTs, highlighting the possible influence of chirality on adsorption processes [77].

Based on the literature reviewed in this chapter, the answer to RQ1 is that CNT–based electrochemical sensors have already been investigated for the detection of E2 in water samples [61, 73, 74]. Many studies report successful detection using

functionalized CNT electrodes, where surface modification is employed to improve sensitivity and selectivity. However, because studies has shown that adsorption is a prerequisite for the electrochemical detection of E2 [60] and evidence also show that SWCNT chirality can influence adsorption interactions [77], it would be beneficial to first understand this phenomenon better for pristine CNTs before adding the functionalization step. It is possible that even pristine CNTs provide sufficiently strong interactions for sensing, and this understanding may also lead to more optimized functionalization strategies.

For this reason, a computational study is conducted to gain a deeper understanding of the atomic-scale phenomena governing the adsorption of E2 on a $(6, 6)$ SWCNT. Using simulations, the aim is to identify the most energetically favorable adsorption configurations and determine the nature of the adsorption interactions between E2 and the $(6, 6)$ SWCNT surface, as addressed in RQs 2 and 3. Ultimately, this knowledge can support the design of more selective and efficient electrochemical sensors for E2 detection.

3 Theoretical Background of Computational Models

Computational materials science is a field that has grown rapidly in recent decades due to the increased availability and reduced cost of high-performance computing platforms. While many of the underlying theoretical frameworks were developed earlier, advances in computational resources have enabled the widespread use of complex computational methods and realistic simulations to address real-world materials problems. As a result, computational materials science has gained increasing potential to contribute to the solution of global technological and environmental challenges [78]. The field focuses on predicting and explaining material properties by simulating their atomistic behavior using theoretical models and numerical algorithms. The knowledge gained from those simulations helps to connect an atomic-scale structure with macroscopic properties, enabling the design and optimization of materials for a wide range of applications.

By using simulations, researchers can reduce the need for costly or resource-intensive experiments while enabling high-throughput screening, rapid prototyping, and predictive modeling [78]. These capabilities support faster innovation in areas such as clean energy technologies, water purification processes, climate-resilient infrastructure, medical diagnostics and monitoring, and circular material design. However, fully realizing this potential requires continued progress in model accuracy, data availability, and systematic validation across multiple length and time scales [78].

Adsorption phenomena represent one class of processes that has been studied computationally [14, 79]. Using computational approaches, adsorption can be modeled at the atomic level, thereby providing insight into adsorption energies, preferred binding sites, surface selectivity, and adsorption mechanisms, which are often difficult to access experimentally. With this knowledge, it is possible to optimize and develop improved materials to enhance adsorption-based processes used in pollutant detection in water samples and other sensing applications.

3.1 Density-functional theory

One widely used computational method in chemistry, physics, and materials science is density functional theory (DFT). DFT is an ab initio quantum mechanical approach used to study the electronic structure of many-body systems [80, 81].

The conceptual origins of DFT can be traced back to the Schrödinger's equation. The equation describes how the wavefunction of a quantum system evolves and determines the physical properties of the material under investigation. Although this equation became one of the basis function of modern quantum physics, solving it exactly for structures with more than one electron proved to be extremely challenging due to interactions between electrons, known as the many-body problem. For example, traditional wavefunction-based methods, such as the Hartree–Fock method, attempt to address this challenge by approximating the many-electron wavefunction of a material. [80, 81] On the other hand, DFT is one of the approaches that address this problem by describing the material in terms of the electron density, which enables the study of more complex atomic and molecular structures.

According to Sholl and Steckel [81], the widely accepted formulation of DFT is based on the two fundamental theorems of Hohenberg and Kohn, which provide the theoretical foundation of the method. In their first theorem, they established that the ground-state energy of a quantum system can be expressed as a functional of

the ground-state electron density $n_0(r)$. Here, a functional refers to a function that accepts another function as an input, in this case the electron density, and returns a single number as an output. The second theorem complements the first by stating that the ground-state electron density is the one that yields the lowest possible value of this energy functional. However, the theorems do not specify the exact form of the functional, and therefore practical calculations rely on approximate expressions.

To address this limitation, Kohn and Sham presented their practical approach to DFT, where the interacting electron system is replaced with a non-interacting reference system and the electron density is obtained using a variational principle [81]. The total energy within the Kohn–Sham framework can be expressed as follows, as presented by Sippola [12]:

$$E_{\mathrm{KS}} = T_s[n] + \int V_{\mathrm{ext}}(r)\, n(r) + E_H[n] + E_{NN} + E_{\mathrm{xc}}[n]$$

where $T_s[n]$ is the kinetic energy of non-interacting electrons, $V_{\mathrm{ext}}(r)$ is the external potential due to nuclei and external fields, $E_H[n]$ is the classical Coulomb (Hartree) energy, E_{NN} is the electrostatic interaction between the positively charged nuclei (NN denotes the total number of nuclei), and $E_{\mathrm{xc}}[n]$ is the exchange–correlation energy, which contains all the electron–electron interaction effects in the model. In the equation, r denotes the spatial coordinate, and $n(r)$ is the ground-state electron density.

The Kohn–Sham method transforms the complex many-body problem to a set of single-electron equations that must be solved self-consistently. It is sufficient to approximate only the exchange–correlation functional $E_{\mathrm{xc}}[n]$, rather than the entire energy functional. [81] This creates an optimization challenge: reducing the computational cost requires the use of approximations, but those approximations inevitably affect the accuracy of the results. As a result, many exchange–correlation functionals exist to balance accuracy and computational efficiency for different types

of materials and properties. The functionals are often arranged according to Jacob's ladder, a conceptual framework in DFT that places them in an order from the simplest to the most accurate [82, 83]. Among these functionals, the Generalized Gradient Approximation (GGA) functional Perdew–Burke–Ernzerhof (PBE) [84] was employed to conduct the calculations in the computational part of this thesis.

GGA functionals occupy the second level of Jacob's ladder. Compared to the simplest level, the Local Density Approximation (LDA) functionals, which assume that the electron density is locally uniform and depends only on its value at each point in space, GGA functionals are more accurate because they account for both the electron density and its gradient at each spatial point. This makes them better suited for real atomic structures where the electron density varies, such as the system studied in this work. At higher levels of Jacob's ladder than GGA are meta-GGA functionals, which add even more information, such as the kinetic energy density, to achieve higher accuracy. Above these are hybrid functionals, which combine the standard DFT exchange functional with a portion of exact Hartree–Fock exchange, improving performance especially for molecular systems. At the top of the ladder are fully nonlocal functionals, which can describe long-range interactions such as vdW forces that lower-level approximations often miss. [82, 83] Despite their higher accuracy, these methods are associated with significantly increased computational cost, making them impractical for calculations involving large systems with hundreds of atoms and requiring extensive sampling. For this reason, GGA provides a good balance between accuracy and computational efficiency for the present system. However, since standard GGA functionals do not accurately describe vdW interactions, many-body dispersion (MBD) corrections were applied in this study to capture these effects [85, 86].

Although DFT is widely used across many research fields and provides advantages such as scalability and compatibility with machine learning approaches, it

also has important limitations [78, 81]. Besides the fact that the accuracy of DFT depends strongly on the chosen exchange–correlation functional, DFT also often struggles with long-range interactions such as vdW forces and tends to underestimate band gaps in semiconductors and insulators [81]. Although DFT is significantly more efficient than wavefunction-based methods, simulations of large and structurally complex configuration models remain computationally demanding. This challenge becomes particularly evident when exploring the potential energy surface (PES) of organic–inorganic interfaces, where many competing structural molecules may exist [13]. Due to the high computational cost of sampling the entire PES, DFT-based studies often rely on reduced or simplified models or evaluate only a limited set of candidate structures based on human intuition [13, 79]. As a consequence, the predicted structures may not fully represent the behavior of real materials. For these reasons, DFT predictions often require validation or correction when applied to real-world materials [78]. In addition, implementing large-scale DFT simulations requires high-performance computing infrastructures with significant energy and cooling demands, raising sustainability concerns.

Compared to classical force-field approaches, which use classical physics instead of quantum mechanics to model interactions, DFT provides an explicit description of the electronic structure, which is essential for accurately modeling adsorption processes. In atomistic simulations, two independent choices must be made: how atomic motion is treated and how interatomic interactions are described. Atomic motion can be studied either through static calculations or optimizations, or through molecular dynamics (MD), which simulates the motion of atoms over time by integrating Newton's equations of motion. The interactions between atoms can be described using classical empirical potentials or using ab initio methods such as DFT. [81] In many DFT studies, the atomic structure is first optimized through a geometry relaxation procedure, meaning that atomic positions are iteratively adjusted until

the forces acting on all atoms fall below a predefined threshold [14, 79, 87]. In adsorption studies the process ensures that the obtained structure corresponds to a local minimum on the PES and represents a physically stable configuration.

Classical MD simulations using empirical force fields allow simulations of large configurations over long time scales, but they cannot explicitly describe electronic effects such as charge redistribution or bond formation, which are central to this study. These effects can be captured using a combination of DFT and MD, but such simulations are computationally expensive and therefore typically limited to relatively small atomic structures and short simulation times. [88]. Because dynamic effects of atoms were not the primary focus and adsorption is governed by electronic interactions, static DFT was employed in this study. It provides a suitable level of theory for analyzing adsorption configurations and interaction energies compared to classical force-field or MD approaches. For example, the electronic structure obtained from DFT can be analyzed using the density of states (DOS), which describes the number of available electronic states at each energy level and provides insight into the distribution of electronic states near the Fermi level. [81] Changes in the DOS upon adsorption can reveal how the interaction between a molecule and a surface modifies the electronic structure of the material. Another useful quantity for analyzing adsorption processes is charge transfer between the adsorbate and the surface, which can be evaluated, for example, using Mulliken charge analysis [89]. This analysis allows the estimation of partial atomic charges, which can provide insight into charge redistribution upon adsorption and the nature of the interaction between the two components.

While static DFT is suitable for capturing such electronic properties, it cannot describe how adsorption may lead to changes in the electronic or optical behavior of a material over time because it represents only a single static configuration. For this reason, time-dependent DFT (TDDFT) [90] has been developed to study elec-

tronic excitation energies and transition probabilities, enabling the investigation of the electronic and optical consequences of surface interactions. However, since the objective of this thesis was to determine possible adsorption configurations of E2, static DFT was considered sufficient for the analysis.

3.2 Bayesian Optimization Structure Search

Various approaches have been developed to integrate machine learning with DFT calculations to enhance simulation speed [91], improve structure prediction [92], and approximate the PES [93]. One such method is Bayesian Optimization Structure Search (BOSS), a relatively recent technique for structure exploration. BOSS applies an active learning approach known as Bayesian Optimization (BO) to improve PES sampling while avoiding systematic bias by adaptively selecting sampling points instead of following a predetermined sampling pattern. It is designed to efficiently explore complex energy and property landscapes by constructing and iteratively refining a surrogate model of the target property. [12, 13, 79]

BO is a probabilistic method used to optimize so-called black-box functions, where the exact mathematical form is unknown, but values can still be evaluated at selected points in the search space. The advantage of BO is that it can find the global minimum or maximum with significantly fewer evaluations compared to traditional methods, making the optimization of computationally expensive functions feasible. [94]

BOSS works in a way that it does not calculate the entire PES of the atomic structure but instead learns its shape iteratively by modeling only the necessary points. It starts with utilizing the BO framework to build from a few DFT-calculated points a predictive surrogate model of the energy landscape, which is typically a Gaussian Process (GP). The model represents the objective function and is updated after each new evaluation using Bayes' theorem, which gradually improves its accuracy.

In each iteration step, the GP produces a prediction consisting of two components: the estimated function value (posterior mean) and the uncertainty of that estimate (posterior variance). Low variance indicates confidence in the prediction, whereas high variance signals uncertainty and the potential for undiscovered optima. The posterior mean and variance are then passed to the acquisition function, which determines the next sampling point by balancing exploration of uncertain regions and exploitation of promising low-energy areas. In this way, BOSS gradually learns the shape of the PES and, once the model has converged, identifies the most stable configuration with as few calculations as possible. [12, 13, 79, 95]

Efficient BOSS exploration relies on representing the structures using a rigid building-block approach, meaning that compounds are treated as rigid units while only their relative positions and orientations are optimized. In this way, the dimensionality of the search space can be reduced, because internal atomic coordinates remain fixed during the search. This is justified, because in molecules containing aromatic rings or stable functional groups such as E2, structural changes during the search are typically limited to small bond adjustments rather than complete rearrangements. This approach accelerates the exploration of large atomic configurations, as it avoids the need to model very small internal variations in the structure. [13] Before carrying out the search, the relevant building blocks and the desired degrees of freedom must be defined based on chemical principles. Once these are set, the algorithm performs the structure search autonomously, ensuring that important configurations are not biased or excluded due to human intuition. However, if the degrees of freedom or building blocks are poorly chosen, internal flexibility in the molecular structure may be overlooked, or the model may produce nonphysical results such as overlapping atoms or unnecessary computational effort [14]. Despite these limitations, BOSS still offers advantages over traditional structure search methodologies. It provides a wide view of the energy landscape,

including both global and local minima, and enables access to multiple energetic and electronic properties within the same workflow. Crucially, BOSS offers significantly higher computational efficiency compared to traditional grid search methods, where all potential parameter combinations must be systematically sampled. Instead, BOSS constructs a surrogate model of the objective function and iteratively selects the most informative sampling points, thereby reducing the number of expensive evaluations required. This makes BOSS a versatile approach for structure optimization, exploration of adsorption configurations, and multi-objective design tasks.

4 Methods for Investigating the Adsorption of E2 on a (6,6) SWCNT

The workflow used in this thesis follows procedures previously described in adsorption studies of organic molecules [12, 14, 79], as illustrated in Figure 4.1. The study consisted of five main phases: (1) structural models of the (6, 6) SWCNT and the E2 molecule were prepared and optimized separately, (2) a Bayesian optimization–based configurational adsorption search was performed to identify potential adsorption configurations, (3) local minima structures were extracted from the search results and relaxed, (4) the relaxed structures were analyzed in terms of their structural properties, and (5) their electronic properties, including the DOS and charge transfer characteristics, were evaluated. The objective of this thesis was to identify the most stable adsorption configurations of E2 on a (6, 6) SWCNT and to determine the nature of the interactions between the molecule and the SWCNT surface.

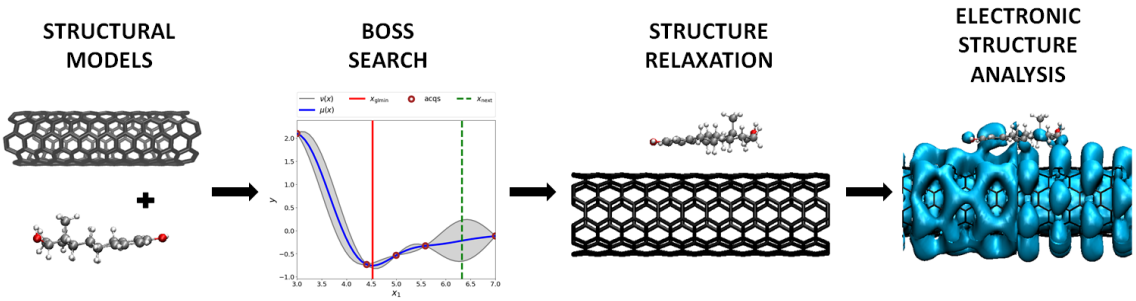

Figure 4.1: Computational workflow used to identify and analyze the lowest-energy adsorption configuration of E2 on a (6, 6) SWCNT.

4.1 Computational implementation

To implement the workflow shown in Figure 4.1, the Atomic Simulation Environment (ASE) [96], the FHI-aims package [97], and the BOSS algorithm [13] were used. ASE is a Python-based toolkit for atomistic simulations, providing tools for constructing atomic structures, manipulating geometries, and analyzing simulations. In this study, ASE was used to construct the initial structure of the $(6, 6)$ SWCNT, generate adsorption configurations, and apply translations and rotations to the E2 molecule relative to the SWCNT surface during the structure search. All DFT calculations were performed using the FHI-aims package (version 240507), which is a computational chemistry software package used to calculate the electronic structure of atoms, molecules, and solids using first-principles methods like DFT. The configurational search was carried out using the BOSS framework [13], interfaced with DFT calculations through a Python user function script. In this setup, BOSS proposed candidate sampling locations at which DFT calculations were performed. The resulting adsorption energies were then returned to BOSS to iteratively update the surrogate model of the energy surface. All calculations were performed using the Finnish national high-performance computing resources provided by CSC – IT Center for Science Ltd.

4.2 DFT calculation settings

The performed DFT calculations, including the optimization of the initial structures, as well as the configurational search, were performed with light default settings and tier 1 basis sets, meaning that less stringent numerical parameters were employed in the calculations. This resulted in lower numerical accuracy during the initial stage of the calculations while significantly reducing the computational cost. To achieve higher accuracy in the analysis phase, stricter numerical parameters were

applied. Therefore, the subsequent refinement and electronic structure analysis were conducted using tight default settings and tier 2 basis sets. The exchange–correlation functional was treated within the generalized gradient approximation using the PBE [84] functional and MBD [85, 86] was employed to account for vdW interactions. All calculations were performed in a spin-unpolarized manner with dipole corrections applied. A $1 \times 1 \times 6$ k-point grid with Gaussian smearing of 0.1 eV was used. A convergence threshold of 10^{-6} eV in total energy change was used as the convergence criterion for the electronic self-consistent field cycle. Structural relaxations were considered converged when the forces on all atoms were below 10^{-3} eV/Å.

The structural models presented in Figure 4.2 were generated separately in the gas phase, meaning that the calculations were conducted in vacuum. The initial structure of the E2 molecule was obtained from a previous adsorption study involving a first-principles structure search of E2 on graphene [12, 14]. In this work, the structure was re-relaxed using MBD vdW corrections, as MBD provides a more accurate description of many-body dispersion effects than the original scheme. The resulting optimized structure served as the input model for the adsorption configuration search. The center of mass (COM) of the E2 model was defined as the origin and used to describe its position relative to the SWCNT surface.

The $(6, 6)$ SWCNT was selected because it has been experimentally studied in the Materials in Health Technology research group at the University of Turku and provides a relatively simple structure compared to other chiralities, making it a suitable starting point for simulation studies. The initial structure of the $(6, 6)$ SWCNT unit cell was generated using the nanotube builder function of the ASE Python package [96]. Periodic boundary conditions were applied to model the system, where the structure is represented by a repeating unit cell. The unit cell parameters, corresponding to the smallest repeating structural unit along the SWCNT axis, were first optimized to obtain the lowest total-energy configuration, followed by relaxation of

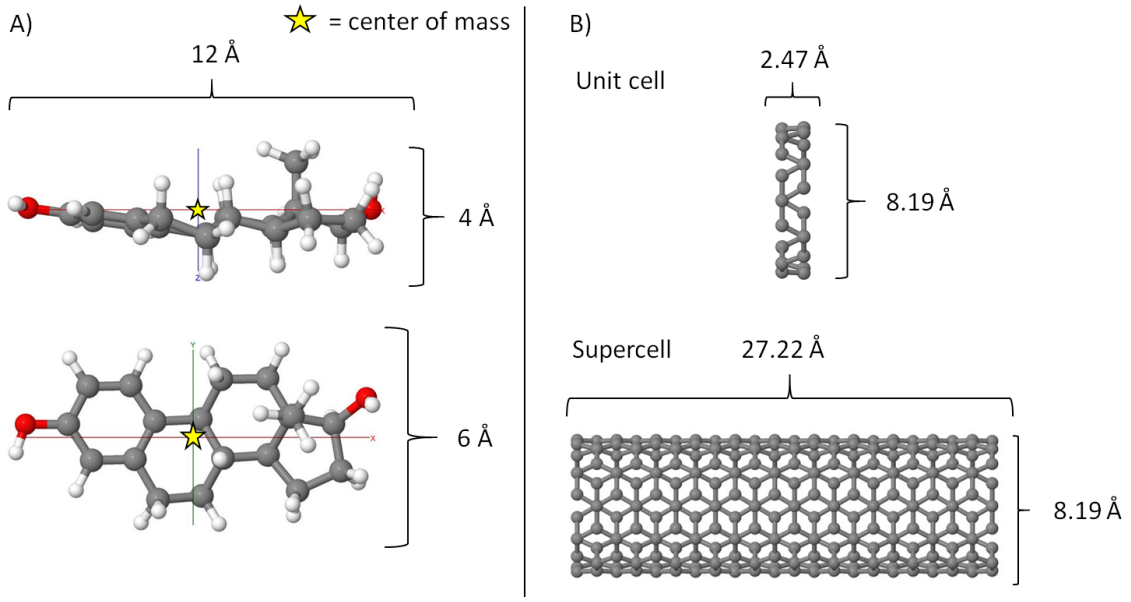

Figure 4.2: Initial structural models generated separately in vacuum. (A) Side and top views of the E2, with characteristic molecular dimensions and the center of mass indicated. (B) Unit cell and supercell models of the (6, 6) SWCNT, including their structural dimensions.

the atomic positions. The relaxed (6, 6) SWCNT structure was characterized by a C–C bond length of 1.429 Å, a unit cell length of 2.47 Å, and a diameter of 8.19 Å. The obtained structural parameters were consistent with previously reported values [70]. To enable the adsorption configuration search, the SWCNT unit cell model was expanded into a supercell, a larger simulation cell constructed by repeating the original unit cell along the SWCNT long axis, because the unit cell length was insufficient compared to the 12 Å backbone length of the E2 molecule, as illustrated in Figure 4.2. The needed supercell was created by repeating the unit cell structure 11 times along the long axis, yielding a input model for structure search with a total length of 27.22 Å, as shown in Figure 4.2. The corresponding lattice vectors were defined as a_1 = [50.0, 0.0, 0.0], a_2 = [0.0, 50.0, 0.0], and a_3 = [0.0, 0.0, 27.220], with the SWCNT long axis aligned along the z-direction. The Cartesian axes were defined as x = [1, 0, 0], y = [0, 1, 0], and z = [0, 0, 1]. A vacuum spacing of 50 Å was introduced in the x and y directions to prevent effects between adjacent SWCNTs.

The adsorption energy of each low-energy configuration was determined from the total energies of the relaxed components using the formula

$$E_{ADS} = E_{TOT} - (E_{SWCNT} + E_{E2}),$$

where E_{TOT} denotes the energy of the combined system after the adsorption, E_{SWCNT} states the energy of the isolated and relaxed $(6, 6)$ SWCNT and E_{E2} is the energy of the isolated and relaxed E2 molecule.

4.3 Structure search

BOSS was interfaced with DFT calculations to perform adsorption structure searches on PES, here referred to as the adsorption energy surface (AES). Each iteration proceeded as follows: (1) BOSS proposed a new sampling point on the AES; (2) the corresponding configuration is generated by translating or rotating the molecule using ASE; (3) a single-point DFT calculation is performed; (4) the adsorption energy is extracted; and (5) the surrogate model of the energy landscape is updated accordingly. This process is illustrated in Figure 4.3.

Certain restrictions on the degrees of freedom were applied to reduce the complexity and computational cost of the search phase calculations. In this approach, the $(6, 6)$ SWCNT and E2 molecules were treated as rigid building blocks, with only their relative positions varied while their internal geometries were kept fixed. It was expected that E2 would preferentially adopt a horizontal adsorption orientation above the SWCNT surface. Previous studies on related aromatic systems, such as dopamine and benzene [67, 98], support this expectation by reporting π–π stacking interactions that favor horizontal adsorption geometries.

The complete adsorption configuration consisting of the E2 molecule above the $(6, 6)$ SWCNT surface was constructed using a Python script that utilized the ASE

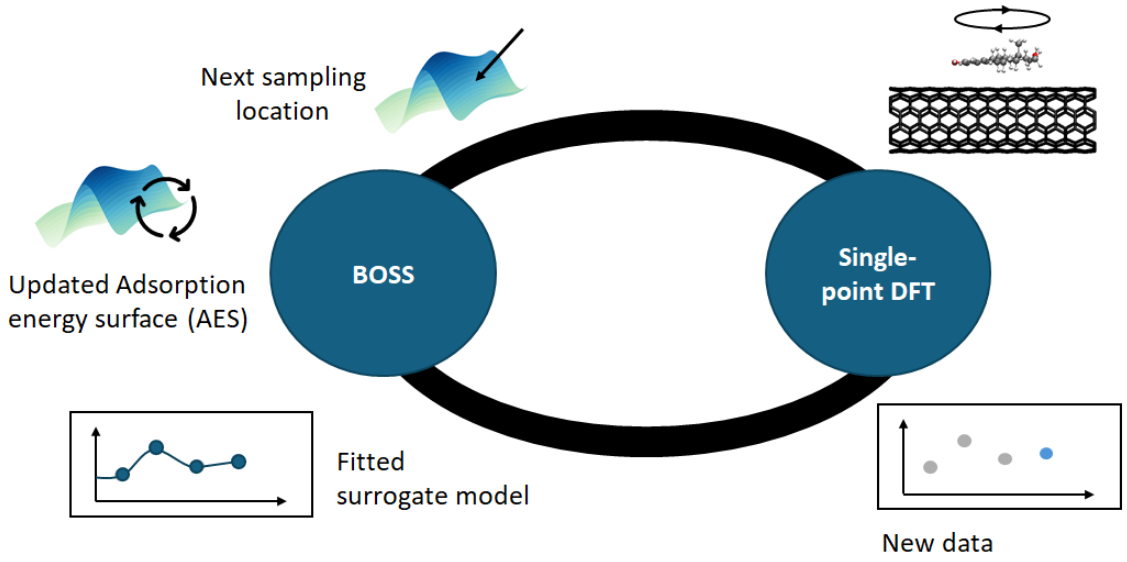

Figure 4.3: Iterative workflow of the BOSS search. Adapted from [11], licensed under CC BY 4.0 (`https://creativecommons.org/licenses/by/4.0/`).

package. The script read the structural information of the $(6, 6)$ SWCNT and the E2 molecule from separate input files and constructed the combined adsorption complex by applying the translations and rotations corresponding to the selected degrees of freedom. At each iteration, the script systematically varied these degrees of freedom to sample different adsorption configurations of the molecule above the SWCNT surface.

Three one-dimensional (1D) BOSS searches were performed before the full four-dimensional (4D) configurational search to evaluate the effect of molecular orientation on adsorption and to determine whether the molecular height above the SWCNT should be fixed to the value that yields the most favorable result in the 1D searches. The tested configurations included the molecular backbone aligned parallel and perpendicular to the SWCNT long axis, with the E2 methyl group oriented away from the SWCNT surface, as well as a parallel orientation in which the E2 methyl group was oriented toward the SWCNT surface. In these searches, only the molecule height above the SWCNT surface (ρ) was allowed to vary during search,

within a range of 3–7 Å. For the configuration in which the methyl group was oriented toward the SWCNT, the range was adjusted to 4–7 Å to prevent the methyl group from coming into contact with the surface at the lower bound of the range. A non-periodic radial basis function (rbf) kernel was employed, with the objective function approximated in the range $[-2, -1]$ eV. Each search was initialized with two Sobol points and the model was updated with 15 new points.

Based on the insights obtained from the 1D searches, the full 4D configurational search was then performed. Four degrees of freedom were allowed to change during the search, which were expected to influence the adsorption energy. These dimensions were the molecule's vertical distance above the SWCNT surface (ρ), the molecule rotation around the SWCNT (ϕ), the molecule's translation along the SWCNT long axis (z), where mirror symmetry was also applied and molecule rotation perpendicular to the surface (γ). The dimensions are illustrated in Figure 4.4.

Periodic boundary conditions were applied to the $(6, 6)$ SWCNT supercell, meaning that the unit cell was periodically repeated in all three spatial directions. Therefore, the search space in the 4D search only needed to cover the coordinates of the smallest repeating unit of the $(6, 6)$ SWCNT: z = 0–2.47 Å and $\phi = 0 - 60°$, where ϕ is the angular coordinate around the tube. The corresponding search space is illustrated in Fig. 4.4 by the red box in panel A). A full 360° search in ϕ is not required because the hexagonal symmetry of the armchair SWCNT causes the atomic structure to repeat periodically around the circumference with a period of 60°. As a result, all symmetry-unique adsorption environments are already represented within a 60° angular interval, which fully captures all distinct adsorption sites around the $(6, 6)$ SWCNT surface. Symmetry along the $(6, 6)$ SWCNT z-axis, illustrated in Figure 4.4 panel A), allows the search space to be reduced. The symmetry line divides the red rectangular search region, meaning that any adsorption point at position z_1 is equivalent to another point at $z_2 = 2.47 - z_1$ within the same unit cell. To

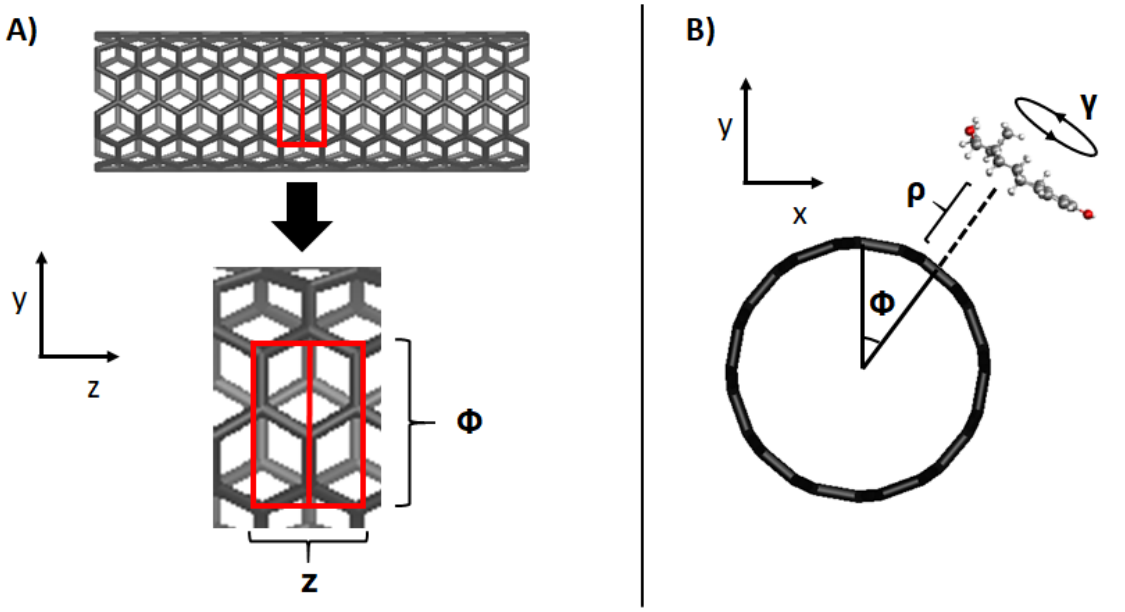

Figure 4.4: Degrees of freedom in the 4D structure search. (A) Side view of a $(6, 6)$ SWCNT illustrating the translation of the molecule along the SWCNT long axis (z) and the rotation around the axis (ϕ). The red rectangle indicates the search space, and the middle line represents the symmetry plane used for the z coordinate. (B) Cross-sectional view showing the vertical distance of the molecule from the SWCNT surface (ρ) and the rotation of the molecule perpendicular to the surface (γ).

exploit this, for every evaluation at z_1, the script manually added a corresponding data point at z_2. In this way, each iteration produced two data points rather than one, effectively doubling the amount of information available to the surrogate model without increasing the number of requested acquisitions. In addition, the rotation of the adsorbate perpendicular to the SWCNT surface was sampled across the full $0 - 360°$ range and the adsorption height (ρ) was restricted to 3.5–6 Å to ensure physically meaningful configurations.

In the 4D search, variables ϕ, z and γ were modeled using the standard periodic (stdp) kernel, while ρ was modeled with a rbf kernel. Parallel optimization was employed to accelerate the calculations on the Mahti supercomputer. The search was initialized with 15 Sobol points and updated with new points selected using the exploratory Lower Confidence Bound (eLCB) acquisition function to guide the

search efficiently [95, 99]. In total, 1163 iterations were completed during the configurational search, corresponding to 2326 evaluated data points when the applied symmetry was taken into account.

After determining the convergence of the structure search, the Broyden–Fletcher–Goldfarb–Shanno algorithm [100] was employed on the 4D adsorption energy surrogate model to ensure that the identified local minima were fully converged during the search. For the application of the algorithm, the methodology presented in the study by Järvi et al. [79] was followed. Using this approach, local minima were extracted approximately every 50–70 iterations, where one iteration was selected for final evaluation.

The resulting candidate minima from selected iteration were analyzed to identify unique low-energy adsorption configurations. Configurations that were duplicates arising from geometrical symmetry related to the periodicity of the $(6, 6)$ SWCNT or from energy variations introduced by the surrogate model were removed. The remaining structures were subsequently subjected to consecutive DFT relaxations, first using light default settings and then refined with tight default settings. During these relaxations, a single carbon atom of the SWCNT was fixed to prevent translational drift.

To examine the relaxed configurations in more detail, key structural metrics were defined, including the adsorption distance, molecular orientation relative to the SWCNT long axis, two different metrics for the adsorption site of the molecule, and the distance of the phenolic oxygen from the SWCNT surface.

The adsorption distance and the phenolic oxygen distance were calculated as the distances between the SWCNT surface and the COM of the E2 molecule and the phenolic oxygen atom, respectively. The molecular orientation was quantified as the angle between the backbone of the E2 molecule and the long axis of the SWCNT, where 0° corresponds to alignment parallel to the SWCNT axis. The backbone of

E2 is defined by the bond between the phenolic oxygen and the adjacent aromatic ring carbon atom. The adsorption site was defined based on the position of the E2 COM relative to the underlying carbon atoms on the SWCNT surface. Three adsorption-site types were considered: 1) top, where the COM is located above a carbon atom; 2) hollow, where the COM is located above the center of a carbon ring; and 3) bridge, where the COM is located above the midpoint of a C–C bond. These site types are illustrated in Figure 4.5. The adsorption site for each configuration was determined by calculating the distances between the E2 COM and all possible adsorption-site reference positions on the SWCNT surface. For each site type, the minimum COM–site distance was identified. A distance threshold of 0.01 Å was applied to account for numerical uncertainty: differences in distances below this threshold were considered negligible, and in such cases the configuration was assigned to multiple possible adsorption sites. Otherwise, the configuration was assigned to the site type corresponding to the shortest distance. To gain further insight into the adsorption position of the E2, the same method was applied to determine the adsorption site of its aromatic ring by evaluating the position of the ring's COM relative to the SWCNT surface.

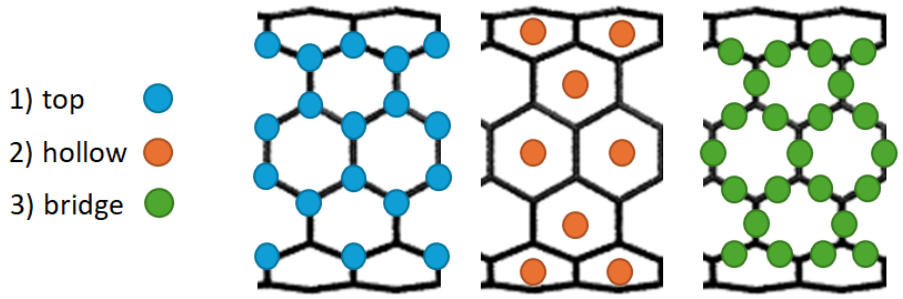

Figure 4.5: Definition of adsorption site types (top, hollow, and bridge) on the $(6, 6)$ SWCNT surface.

Additional structural metrics were evaluated to assess the effects of adsorption on the SWCNT and the internal structure of the E2 molecule. The root-mean-square deviation (RMSD) of the molecule was calculated by comparing each configuration to

the global minimum adsorption structure in order to quantify structural differences between configurations. To assess possible $(6, 6)$ SWCNT distortions, the RMSD of the SWCNT carbon atoms was calculated by comparing atomic positions between the isolated SWCNT gas-phase structure and the relaxed adsorption configurations. In addition, the radial distances of the carbon atoms from the SWCNT central axis were analyzed, and their standard deviation and minimum–maximum range were evaluated to characterize structural variations between adsorbed configurations.

Finally, electronic structure analyses were conducted by calculating the DOS and the partial density of states (pDOS). The pDOS represents the contribution of specific atoms or components to the total electronic states, allowing investigation of how E2 and the $(6, 6)$ SWCNT individually contribute to the overall electronic structure. Furthermore, the highest occupied molecular orbital (HOMO) and lowest unoccupied molecular orbital (LUMO) were visualized. Molecular orbitals describe the spatial distribution of electrons in a system, with the HOMO corresponding to the highest-energy occupied state and the LUMO to the lowest-energy unoccupied state. These frontier orbitals provide insight into regions of electron donation and acceptance and are therefore useful for assessing charge transfer and electronic interactions between the molecule and the SWCNT. In addition, Mulliken charge analysis was performed to investigate how adsorption affects the electrical properties of the systems, such as charge transfer, which has a direct impact on sensing performance.

5 Results

In this chapter, the results of the structure search are presented to identify the most stable adsorption configurations and to gain insight into the interactions between E2 and the $(6, 6)$ SWCNT. The results of the preliminary 1D searches are first introduced, as they were used to determine appropriate bounds for the adsorption height (ρ). Since these limits were not obvious beforehand, unlike for the other variables, representative edge cases were examined to guide their selection.The convergence of the 4D search is then described by presenting the adsorption energy landscapes and the global minima prediction plots. The determination and extraction of local minima candidates are also described, followed by a discussion of the number of configurations identified within the considered energy range. Finally, the identified local minima structures are examined in detail through structural analysis using geometric metrics, including the spatial orientation, position, and distance of the adsorbed molecule relative to the SWCNT surface. In addition, the configurations are investigated through electronic structure analysis to gain deeper insight into how adsorption affects both the molecule and the SWCNT, and to identify the key interactions governing the adsorption process.

5.1 Results of the preliminary 1D BOSS search

The results of the 1D structure searches are presented in Figure 5.1, while the processed data are summarized in Table 5.1. The adsorption energy profiles illustrate

how the energy varies as a function of the adsorption height (ρ) for different molecular orientations. These searches were performed to determine appropriate bounds for the adsorption height (ρ), which was not known a prior and therefore required preliminary evaluation. The lowest energy was obtained for the configuration in which the methyl group points away from the SWCNT surface and the molecular backbone is aligned parallel to the SWCNT long axis, yielding a minimum adsorption energy of -0.73 eV at a height of 4.4 Å above the SWCNT.

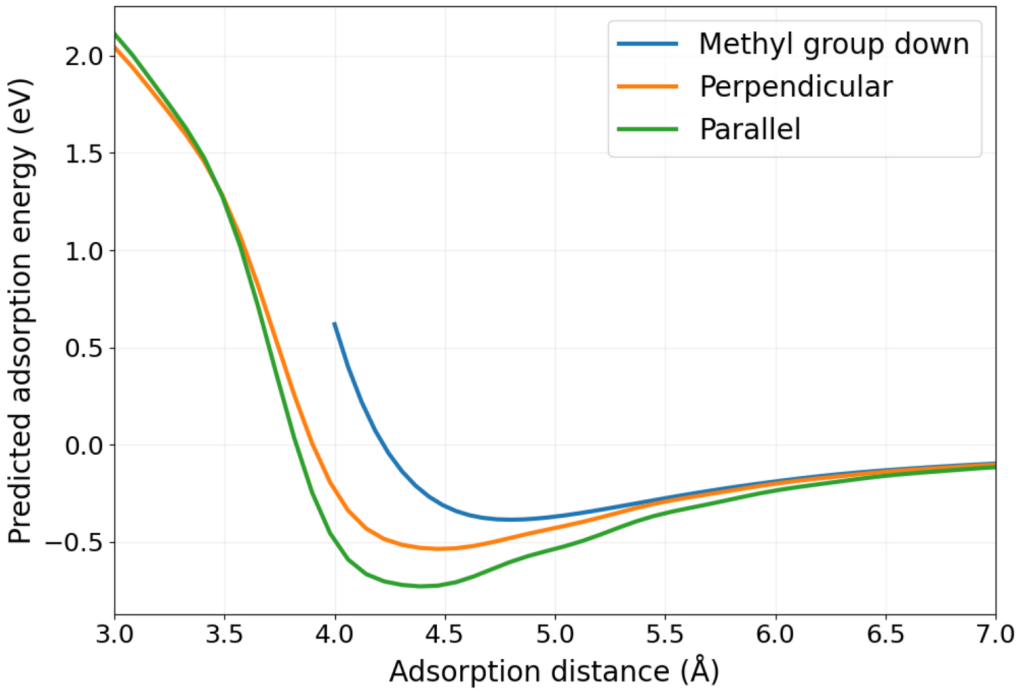

Figure 5.1: Adsorption energy profiles obtained from 1D searches for three molecular configurations. The y-axis shows the predicted adsorption energy (eV), and the x-axis represents the adsorption distance (Å).

Based on these results, ρ was not fixed in the subsequent 4D searches. As shown in Figure 5.1, the adsorption energy profiles for the perpendicular and parallel configurations exhibit minima at slightly different ρ values, with the lowest energies generally occurring in the range of approximately 4–5 Å. This variation indicates that fixing ρ to a single value could exclude favorable configurations, why it was allowed to vary within a reduced range of 3.5–6 Å in the 4D searches, narrowed

from the initial 3–7 Å range used in the 1D calculations. The range was selected to include all observed energy minima while excluding regions at shorter and longer distances where the adsorption energies are consistently higher.

Table 5.1: Predicted optimal adsorption distances and energies for different E2 orientations on a $(6, 6)$ SWCNT obtained from the 1D BOSS search.

Orientation above SWCNT	**Distance (Å)**	**Adsorption energy (eV)**	**Structure**
Parallel	4.40	−0.73	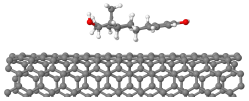
Perpendicular	4.48	−0.54	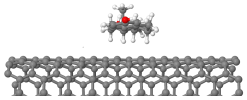
Methyl group down	4.80	−0.39	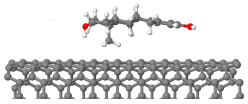

The configuration with the methyl group oriented toward the SWCNT surface was excluded from the subsequent 4D BOSS searches because the 1D results showed clearly weaker adsorption energy compared to the alternative orientations, as shown in Figure 5.1 and in Table 5.1. This orientation was unlikely to produce low-energy configurations in the 4D search and was therefore omitted to focus the exploration on the most relevant regions of the configurational space.

5.2 Convergence of the 4D BOSS search

To assess the convergence of the structure search, the global minimum prediction plot, which visualizes the predicted minimum adsorption energy at each iteration, was first examined. The plot from the 4D search, illustrated in Figure 5.2, showed a trend toward convergence after approximately 300 iterations, but additional lower minima were still identified around iteration 1000. Before increasing the number of iterations, other indicators were also examined to evaluate convergence.

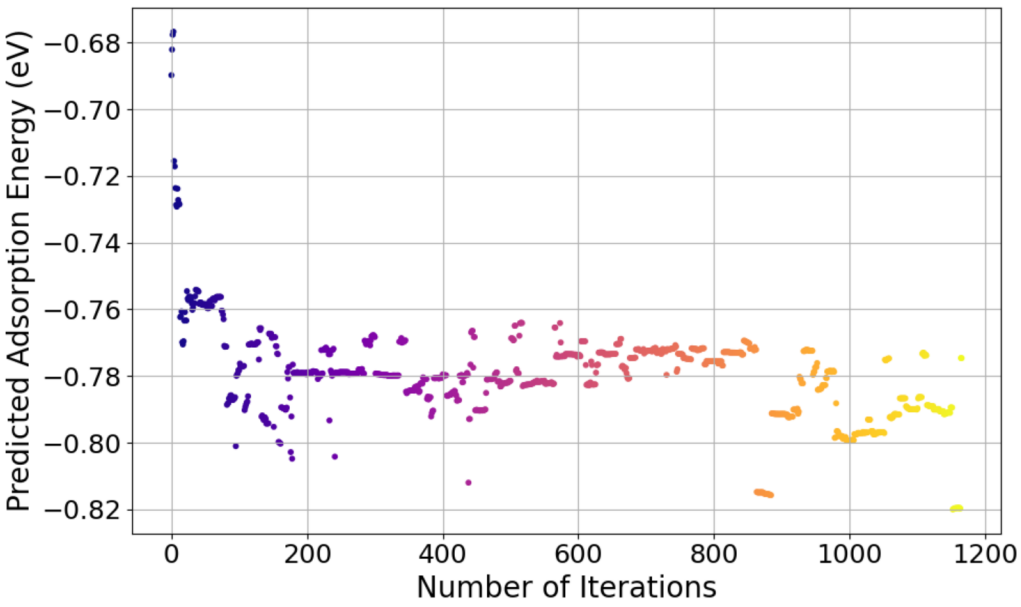

Figure 5.2: Predicted global minimum adsorption energy as a function of iteration during the 4D BOSS search. The y-axis shows the adsorption energy (eV), and the x-axis represents the number of iterations.

Next, the kernel lengthscales were plotted. These hyperparameters of the GP model reflect how sensitively the predicted adsorption energy responds to changes in the input variables. Stable values indicate that the model's sensitivity to the input variables has stabilized. The kernel lengthscales of the 4D search are illustrated in Figure 5.3. As can be seen from the figure, the lengthscale of the z variable exhibits significant fluctuations between low and high values, whereas the lengthscales of the other variables remain relatively stable in the low-value region, indicating convergence. The fluctuations in the z variable affect the smoothness and reliability of the energy landscape. Therefore, the evaluation of adsorption configurations was restricted to regions where the z related kernel parameters, such as the kernel lengthscale, remained less than or equal to two. This criterion was chosen to ensure that the lengthscale of the z variable was comparable to those of the other degrees of freedom, indicating similar sensitivity across all variables.

Despite fluctuations in the kernel parameters, the two-dimensional energy landscapes shown in Figure 5.4 display consistent features across iterations. In the figure,

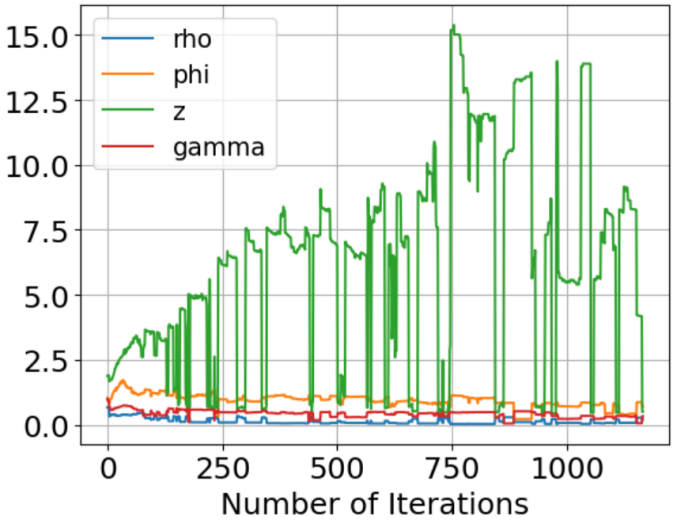

Figure 5.3: Kernel lengthscales of the degrees of freedom as a function of iteration during the 4D BOSS search. The x-axis represents the number of iterations, and the y-axis shows the kernel lengthscale values.

the color scale represents the adsorption energy: darker blue regions correspond to lower energies and lighter colors indicate higher energies. As shown in Figure 5.4, the dark blue regions appear at nearly identical locations in both iterations, indicating that the model reliably identifies the same favorable adsorption regions with similar adsorption energy magnitudes. The comparable color scales in both iteration further support the consistency of the predicted energy ranges.

In addition, the local minima plots, illustrated in Figure 5.5, showed repeated patterns across multiple iteration windows, indicating that similar adsorption energy levels were consistently identified during the search. In particular, the plateaus observed in the low-energy region are closely aligned across different iterations, providing evidence that the optimization repeatedly converged to similar local minimum configurations. Based on this assessment, the structure search was considered sufficiently converged for analytical purposes.

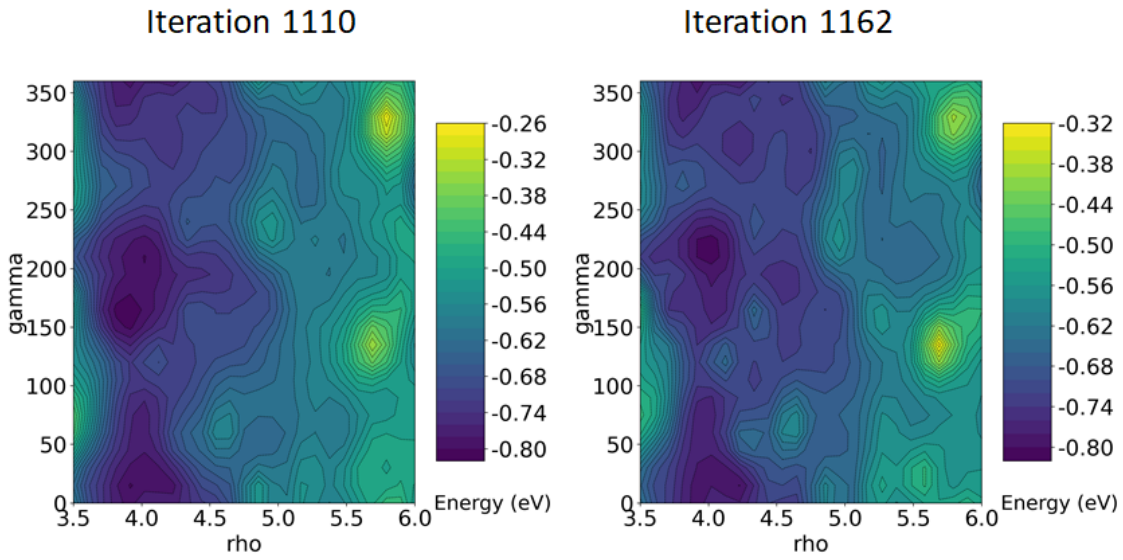

Figure 5.4: Two-dimensional adsorption energy landscapes as a function of ρ and γ at two BOSS iterations (1110 and 1162). The x-axis represents ρ, the y-axis represents γ, and the color scale indicates the adsorption energy (eV). The similarity of the landscapes at the two iterations indicates convergence of the search.

5.3 Local minima identification

Following the convergence of the 4D structure search, the local minima of the AES were refined using the procedure described in Chapter 4. Candidate local minima, shown in Figure 5.5, were obtained at intervals of approximately 50–70 iterations during the structure search (iterations 565, 665, 740, 850, 940, 970, 1055, 1110, and 1162). These intervals were selected to investigate the identification of local minima throughout the search process and because they correspond to regions where the kernel lengthscale of the z variable were comparable to those of the other variables, indicating a stable model response.

During the extraction of local minima information, difficulties arose due to the implementation of the user-defined symmetry function in the code. With the use of this function, symmetry-equivalent configurations were manually written as separate entries in the output file for each resulting data point, leading to duplicate entries. As additional iterations were performed, the code was not able to correctly handle these

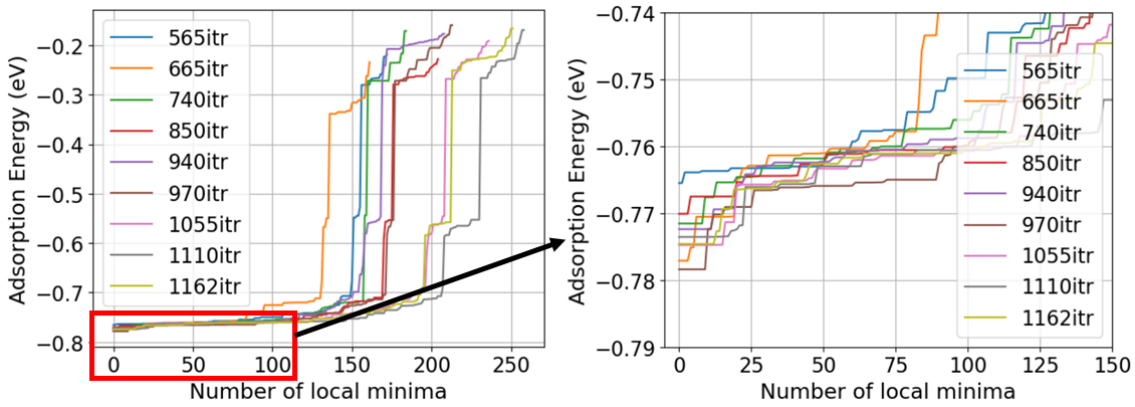

Figure 5.5: Adsorption energies of identified local minima for different BOSS iterations. The x-axis represents the number of local minima, while the y-axis shows the corresponding adsorption energy (eV). The right panel shows a zoomed-in view of the lowest-energy region.

duplicated entries, which resulted in inconsistencies in indexing during the post-processing step. The issue was addressed during the analysis phase by developing a function to extract the correct index corresponding to each iteration, ensuring consistent mapping of the data. This issue affected only the identification of the correct iteration index during data extraction and did not impact the final results.

Figure 5.6 presents the two-dimensional energy landscapes obtained from 1162nd BOSS iteration.. Both landscapes reveal multiple distinct local minima, highlighted by the red circles. These minima correspond to the dark blue regions, which indicate the lowest energy values on the color scale. In the z–ϕ landscape (panel a), two minima are observed at approximately $\phi = 50°$, with $z \approx 0.2$ Å and $z \approx 2.2$ Å. Higher-energy regions appear in the middle of the landscape. In the ρ–γ landscape (panel b), three deep minima are identified in regions where $\rho \approx 4$ Å. Higher-energy regions occur at larger ρ values, particularly above approximately 5.2 Å. This indicates that ρ has a stronger influence on the adsorption energy than γ, which is consistent with the trends observed in the 1D adsorption energy profiles.

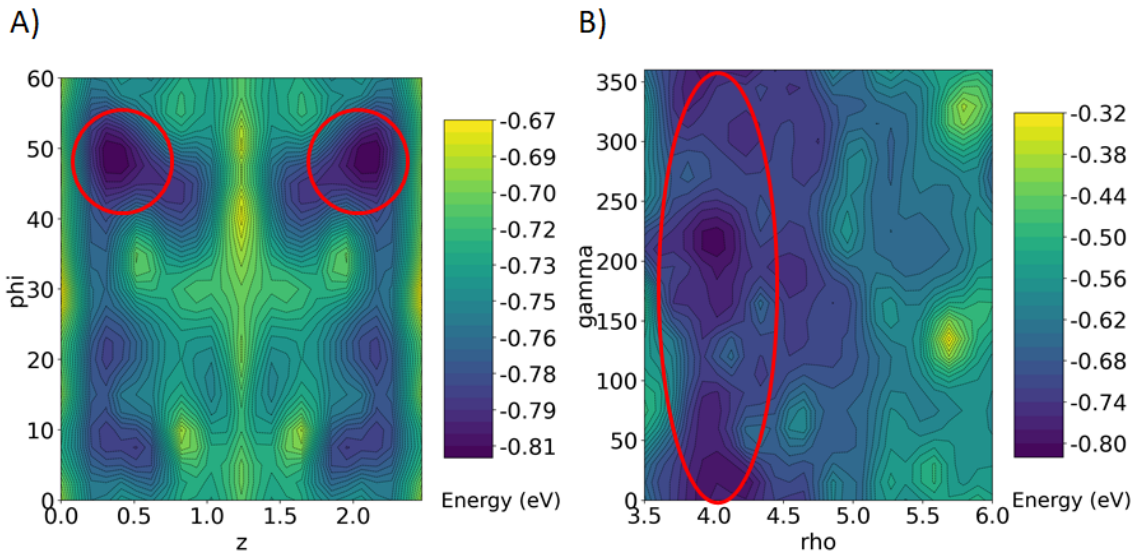

Figure 5.6: Two-dimensional cross-sections of the adsorption energy landscape obtained from the 1162nd BOSS iteration. (a) z–ϕ cross-section. (b) ρ–γ cross-section. The lowest-energy regions are highlighted by red contours.

To identify the most relevant adsorption configurations, local minima were analyzed within an energy range defined by kT, the thermal energy at room temperature. At room temperature, molecules can diffuse between different configurations within the kT range without requiring additional external energy. For this reason, configurations within this energy range were investigated to identify all possible structures at room temperature. Starting the local minima identification from the dataset obtained at the 1162nd iteration, the first post-processing step involved the removal of duplicate structures within kT energy range, based on similarities across the four degrees of freedom. In Figure 5.5, duplicate configurations are located on the same or nearby energy plateaus, indicating that they correspond to nearly identical energies and geometries. After that, all remaining structures were visualized and additional near-duplicates were discarded. These duplicates were not always detectable from the numerical values alone, as some configurations differed by 30° in ϕ while still resulting in the same physical structure. This was due to the periodicity of the ϕ coordinate around the long axis of the $(6, 6)$ SWCNT. Structures that

were similar but had higher energies were also discarded, as these were deemed artifacts caused by fluctuations in the surrogate model. After the full filtering process, 15 BOSS-predicted structures remained that were mutually distinguishable. Relaxation of these structures revealed that one of them relaxed into the same geometry as another minimum. The final dataset therefore contained 14 unique structures, which were then examined with respect to their structural features and electronic properties.

5.4 Structural analysis

In this section, the 14 resulting configurations are first analyzed using the defined structural metrics in Chapter 4 and classified into different structural types. Subsequently, the corresponding energetics are presented, and the features of the identified groups are compared.

Most of the resulting structures were relatively similar, as the E2 molecule does not possess substantial internal flexibility and therefore behaves largely as a rigid aromatic structure. As a result, the main differences between the identified configurations arise from the adosprtion energy, the molecular orientation relative to the $(6, 6)$ SWCNT long axis, the adsorption distance from the SWCNT surface and the phenolic oxygen distance from the SWCNT surface. Additional descriptors include the adsorption site of the molecule based on the E2 COM, and the adsorption site of the aromatic ring COM, which was analyzed separately to better capture the local adsorption behavior of the molecule above the surface. These six descriptors were therefore used as the primary metrics to distinguish the structures into different groups.

Among the relaxed structures, the adsorption distance varied only slightly, ranging from 3.72 Å to 3.80 Å, as illustrated in Figure 5.7. This small variation indicates that the molecule generally remains at a similar height above the surface.

As shown in Figure 5.7, structures with larger adsorption distances correspond to higher adsorption energies, while shorter distances are associated with lower-energy configurations.

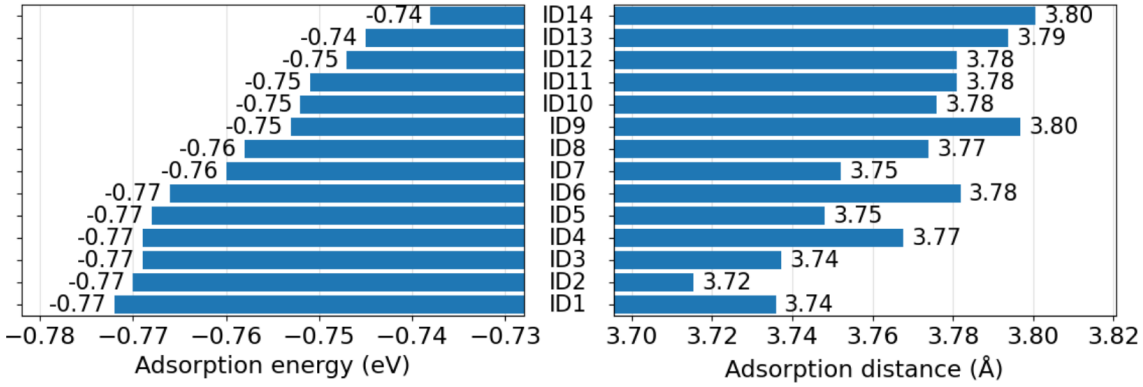

Figure 5.7: Adsorption energies (left) and adsorption distances (right) for the identified local minimum configurations obtained from the 4D BOSS search. The y-axis lists the configuration identifiers, while the x-axes represent adsorption energy (eV) and adsorption distance (Å), respectively.

In contrast, the molecular orientation relative to the long axis of the $(6, 6)$ SWCNT showed more significant variation, as illustrated on the left side of Figure 5.8. Larger rotation angles correlated with lower adsorption energies. An angle of approximately 18° produced the most favorable orientation, whereas the smallest angles were observed in the highest-energy structures. The phenolic oxygen distance was analyzed to quantify structural changes of E2 upon adsorption, where the molecular backbone appeared to flatten compared to the gas-phase configuration. The shift toward the surface was on average approximately 0.5 Å across all identified configurations relative to the gas phase. The variation in distance between configurations was small, with only 0.24 Å separating the minimum and maximum values. As shown on the right side of Figure 5.8, configurations with lower adsorption energies exhibited larger phenolic oxygen distances, whereas higher-energy configurations showed shorter distances, indicating that the phenolic oxygen atom is positioned closer to the SWCNT surface.

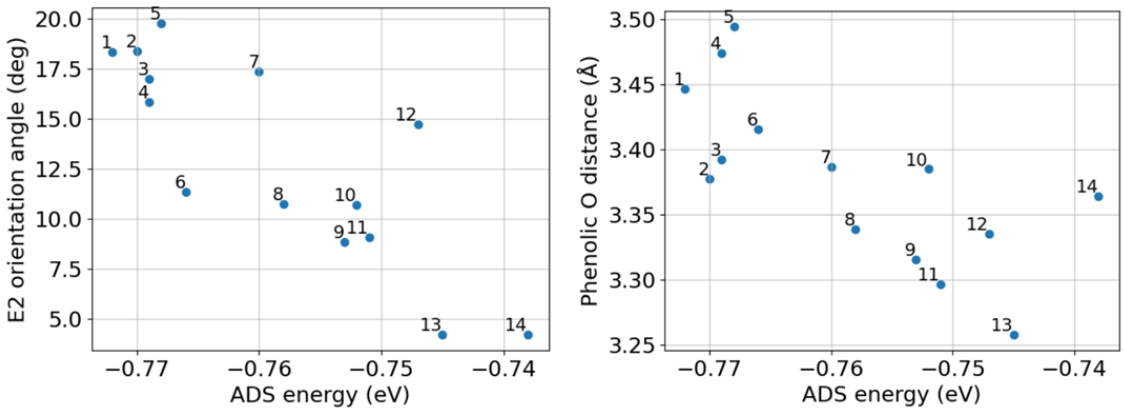

Figure 5.8: Adsorption energy as a function of (left) E2 orientation angle and (right) phenolic oxygen distance from the SWCNT surface for the identified local minimum-energy configurations. The x-axis represents the adsorption energy (eV), while the y-axes show the E2 orientation angle (deg) and phenolic oxygen distance (Å).

The adsorption sites of the configurations were analyzed using the approach defined in Chapter 4, in which the minimum distance between the E2 COM and the candidate adsorption sites was calculated. The hollow site was the most favored position across both low- and high-energy configurations. Only two structures preferred the bridge site, while three structures favored the top site. These structures were located in the middle of the adsorption energy range among the fourteen identified configurations. For some configurations, the distinction between preferred adsorption sites was not clear, as the differences in distances between candidate sites were very small. In such cases, multiple adsorption-site assignments were obtained based on the applied distance threshold. To gain further insight into the adsorption behavior of the whole molecule, the same method was also applied to determine the adsorption site of its aromatic ring, in order to assess whether configurations with the same E2 COM-based adsorption site differ in terms of the adsorption site of the aromatic ring.

By combining these metrics, three distinct structural groups were identified to facilitate comparison between configurations with similar geometric characteristics

and to analyze their relationship with adsorption energy. All identified adsorption configurations, along with their structural metrics and groupings, are presented in table 5.2. The configurations are labeled in order of increasing adsorption energy.

Table 5.2: Identified local minimum-energy adsorption configurations of E2 on a $(6, 6)$ SWCNT and their key metrics, including configuration ID, adsorption energy E (eV), adsorption distance (Å), E2 molecular orientation angle (°), adsorption site of the E2 center of mass (COM) adsorption site of the aromatic ring COM, phenolic oxygen distance (Å), and structural group classification. The configuration IDs are assigned in order of increasing adsorption energy.

	Adsorption		E2 orient.	Adsorption site		Phenolic O	Structural
ID	E (eV)	dist. (Å)	angle (°)	E2 COM	arom. ring	dist. (Å)	group
1	-0.772	3.736	18.338	hollow	bridge	3.446	1
2	-0.770	3.715	18.379	hollow	bridge	3.377	1
3	-0.769	3.737	17.006	hollow	bridge	3.392	1
4	-0.769	3.768	15.849	hollow	top/bridge	3.474	1
5	-0.768	3.748	19.788	bridge	bridge	3.494	1
6	-0.766	3.782	11.355	hollow	top	3.415	1
7	-0.760	3.752	17.392	hollow	top	3.386	1
8	-0.758	3.774	10.735	top	bridge	3.339	2
9	-0.753	3.797	8.829	bridge	top	3.315	2
10	-0.752	3.776	10.673	top	hollow	3.385	2
11	-0.751	3.781	9.086	top	top	3.296	2
12	-0.747	3.781	14.748	hollow	top	3.335	2
13	-0.745	3.794	4.201	hollow	bridge	3.258	3
14	-0.738	3.801	4.198	hollow	hollow	3.364	3

Structural Group 1 Structural Group 1 contained seven configurations, which were configurations located on the lower-energy side of the energy range, with adsorption energies ranging from approximately -0.77 to -0.76 eV. They exhibited relatively large long axis orientation angles, ranging from 11.36° to 19.79°, and short adsorption distances below 3.78 Å, with the smallest distance being 3.715 Å. The adsorption site of the molecule's COM was the same for all configurations in this group, corresponding to a hollow site. For the aromatic ring, the bridge site was

most commonly observed, although a few configurations also exhibited the top site. The phenolic oxygen distance from the surface in this group ranged from 3.38 Å to 3.47 Å, representing the largest distances among all configurations.

The most lowest energy adsorption configuration belonged to Structural Group 1. In this global minimum structure, presented in Figure 5.9, the adsorption distance was 3.736 Å, and the long axis orientation angle was 18.3°. The molecule's COM was positioned above a hollow site, while the COM of the aromatic ring lay above a bridge site. The corresponding adsorption energy was −0.772 eV.

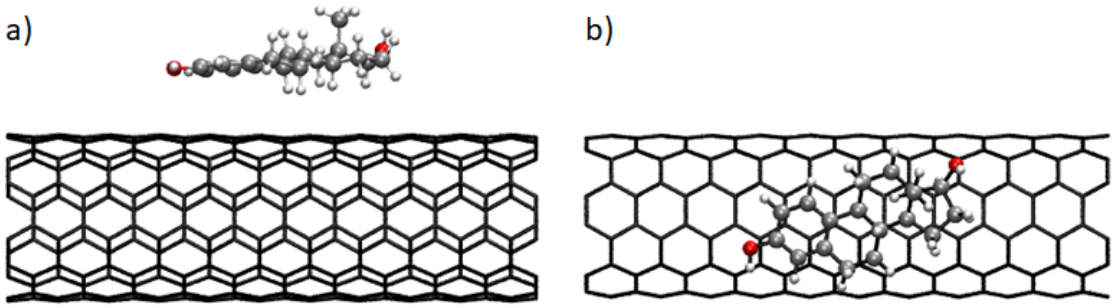

Figure 5.9: Lowest-energy adsorption configuration of E2 on a $(6, 6)$ SWCNT (structure ID 1). (a) Side view and (b) top view of the adsorbed configuration. For clarity, the back side of the SWCNT is omitted in view (b).

Structural Group 2 Structural Group 2 consisted of five configurations. An example configuration from this group is presented in Figure 5.10. The adsorption energies in this group ranged from approximately −0.76 to −0.75 eV, placing them in the middle of the overall observed adsorption energy range. The configurations in the group 2 exhibited adsorption distances within a narrow range (3.75–3.76 Å), and the long axis orientations were relatively similar across the group (8.8°–14.7°). For both the E2 COM and the aromatic ring, the top site was the most common adsorption site. The phenolic oxygen distance ranged from 3.30 to 3.39 Å, which is smaller than in Group 1, indicating that in this group the phenolic oxygen is positioned closer to the SWCNT surface.

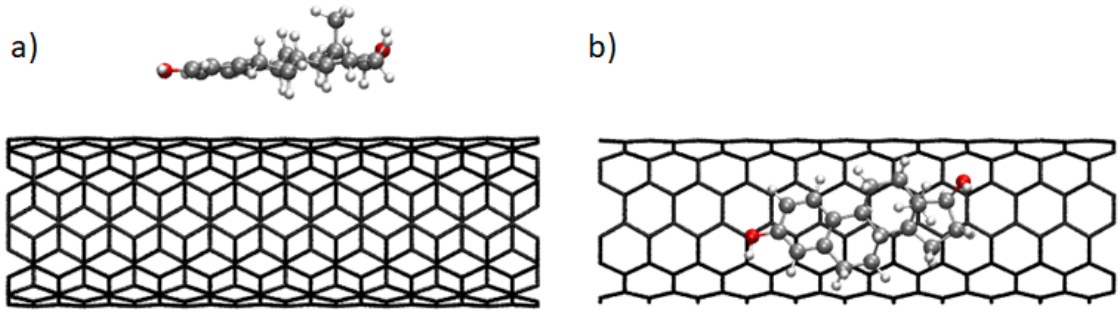

Figure 5.10: Adsorption configuration of E2 in structural group 2 (structure ID 8) on a $(6, 6)$ SWCNT. (a) Side view and (b) top view of the adsorbed configuration. For clarity, the back side of the SWCNT is omitted in view (b).

Structural Group 2 differed from the Group 1 most clearly in terms of adsorption sites and molecular orientation. In Group 1, the adsorption site of the E2 COM was typically a hollow site, whereas in Group 2 a top site was favored. In addition, the combination of adsorption sites for the E2 COM and the aromatic ring showed greater variation than in the other groups. In addition, the molecular orientation angles were also smaller compared to Group 1.

Structural Group 3 Structural Group 3 contained two configurations, one of which is illustrated in Figure 5.11. The distinguishing characteristics of this group were the small molecular orientation angles, the highest adsorption energies, and the largest adsorption distances, indicating that this group corresponds to the most weakly bound structures. The adsorption energies ranged from -0.75 to -0.74 eV, representing the highest values among all configurations, and adsorption distance was approximately 3.80 Å for both configurations. The observed orientation angles were approximately 4.2° for both configurations, representing the smallest values among all identified structures and indicating that the molecules were nearly parallel to the SWCNT long axis. In contrast, the phenolic oxygen distance ranged from 3.26 to 3.36 Å, which is smaller than in the other groups, indicating that the phenolic oxygen is positioned closer to the SWCNT surface. For both configurations, the

molecule's COM was adsorbed at a hollow site, while the adsorption site of the aromatic ring was bridge for one structure and hollow for the other.

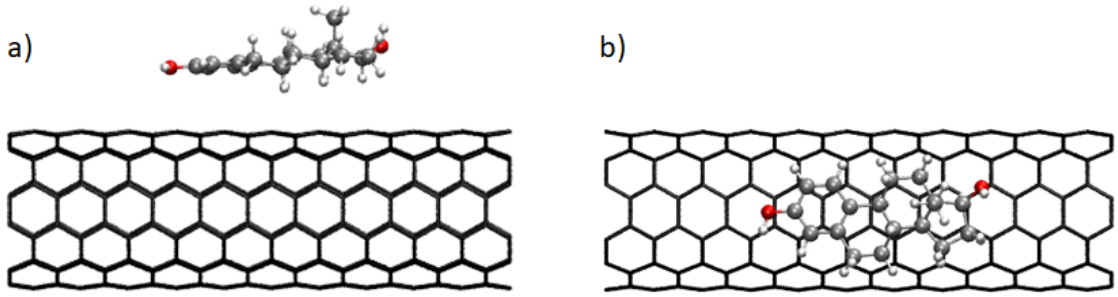

Figure 5.11: Adsorption configuration of E2 in structural group 3 (structure ID 13) on a $(6, 6)$ SWCNT. (a) Side view and (b) top view of the adsorbed configuration. For clarity, the back side of the SWCNT is omitted in view (b).

As mentioned in Chapter 4, additional metrics were calculated to assess the effects of adsorption on both the $(6, 6)$ SWCNT and the internal structure of the E2. The RMSD values of the E2 relative to the global minimum adsorption structure were small, indicating only minor structural differences and limited internal rearrangement. This reflects the relatively rigid nature of E2, which has limited internal degrees of freedom. Moreover, since the building-block method was used and the molecule was treated as rigid during structure generation, the observed RMSD differences mainly arose during the subsequent relaxation steps.

Similarly, the RMSD of the $(6, 6)$ SWCNT carbon atoms showed small deviations between the isolated and adsorbed structures. The radial distances of the carbon atoms from the SWCNT central axis also exhibited only minor variations, as reflected in their standard deviation and minimum–maximum range. Although these changes are small, only on the order of 0.01 Å, the non-zero RMSD values and measurable variations in radial distances indicate that slight structural deformations occur in the SWCNT upon adsorption. A more targeted analysis focusing exclusively on the carbon atoms located directly beneath the adsorbed molecule could provide clearer insight into the extent of local surface deformation.

5.5 Electronic structure analysis

Electronic structure analysis was conducted for selected adsorption configurations to investigate how adsorption affects the electronic properties of the $(6, 6)$ SWCNT–E2 system. One representative configuration from each structural group was selected, corresponding to ID 1, ID 8, and ID 13. For these configurations, the total DOS and the pDOS of E2 and the $(6, 6)$ SWCNT were calculated. In addition, Mulliken charge analysis was performed, and the HOMO and LUMO of the system were visualized to further clarify charge distribution, electronic interactions, and changes resulting from adsorption.

The electronic structure analysis was initiated with the global minimum configuration (ID 1). From the total DOS of the system and the pDOS contributions of E2 and the $(6, 6)$ SWCNT, presented on the left side of Figure 5.12, it can be concluded that the electronic states of the SWCNT dominate the overall electronic structure. The continuous pDOS of SWCNT across the Fermi level reflects the metallic nature of the $(6, 6)$ SWCNT. In contrast, the pDOS contribution from E2 is relatively small and does not introduce new electronic states near the Fermi level but instead modifies existing ones. In particular, adsorption of E2 affects the energy levels below the Fermi level, as evidenced by a shift in the HOMO position in the low-energy region of the total DOS on the left side of Figure 5.12.

The other selected configurations exhibit the same qualitative behavior in both DOS and pDOS, as observed for structure ID 1 on the left side of Figure 5.12. Overall, these results indicate that adsorption does not substantially alter the electronic structure of either component. This suggests that the interaction is weak and consistent with a physisorption mechanism rather than covalent bond formation.

Further insights were gained from visualization of the HOMO and LUMO of the system, as shown on the right side of Figure 5.12. Visualization of the HOMO reveals partial overlap between molecular orbitals and the surface states of the SWCNT

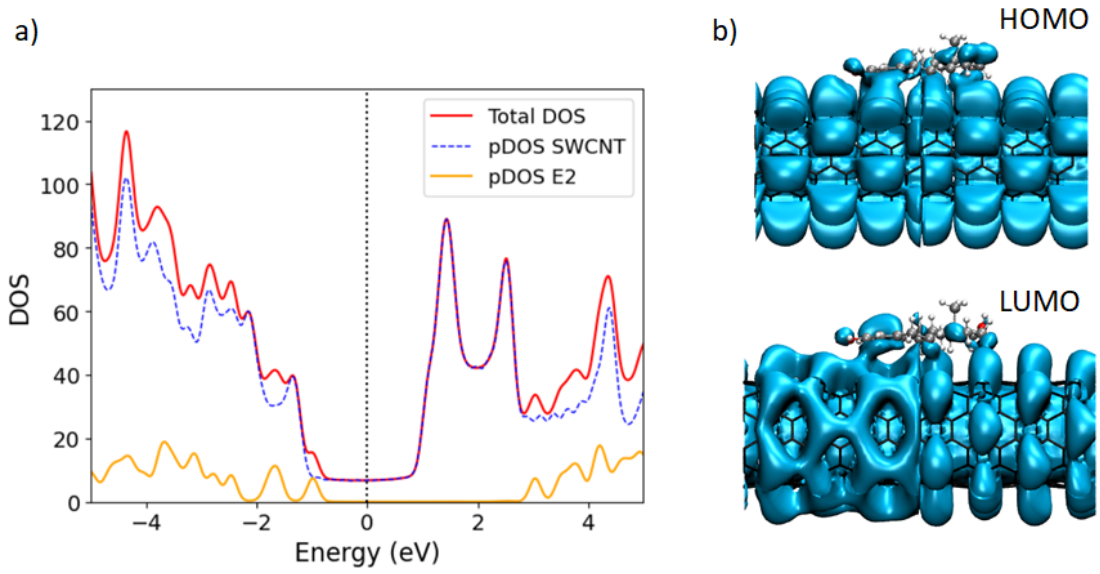

Figure 5.12: Electronic structure of E2 adsorption on a $(6, 6)$ SWCNT (structure ID 1). (a) Total DOS of the system and pDOS contributions from E2 and the SWCNT as a function of energy (eV). (b) HOMO and LUMO of the system, plotted at an isosurface value of 0.001 e Å^{-3}.

along the length of the molecule. A similar type of overlap is observed for the LUMO, with stronger overlap localized on the left side of the molecule, where the aromatic ring is. Additionally, beneath the aromatic ring, the electronic state distribution of the SWCNT exhibits a well-defined honeycomb lattice pattern, whereas regions not located beneath the aromatic ring exhibit more diffuse, point-like electronic features rather than a continuous lattice structure. In comparison, the LUMO of the pristine SWCNT (Figure 5.13) exhibits a more point-like electronic distribution, similar to the regions not located beneath the aromatic ring. This indicates that adsorption affects the electronic states, leading to a more connected distribution and a more clearly defined honeycomb lattice pattern beneath the aromatic ring in the case of structure ID 1.

To further identify the nature of the forces governing the molecule–surface interaction, Mulliken charge analysis was performed to quantify charge transfer between the molecule and the SWCNT. The calculated charge transfer was very small,

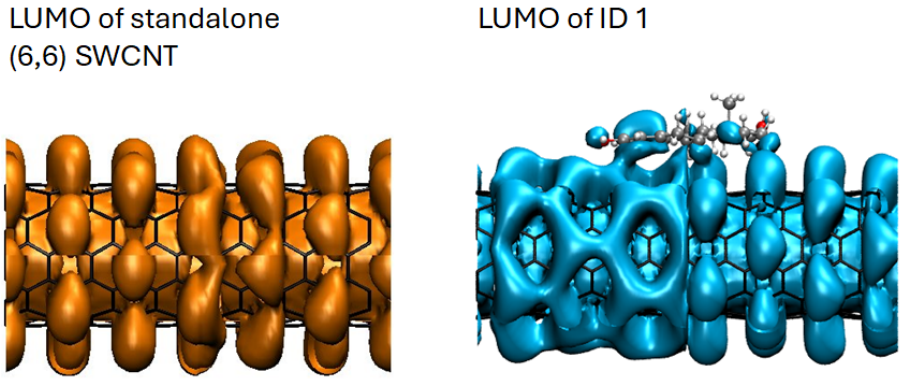

Figure 5.13: Visualization of the LUMO of of a standalone $(6, 6)$ SWCNT (left) and the adsorbed system (structure ID 1, right). LUMO of the system is plotted at an isosurface value of 0.001 e Å^{-3}.

amounting to only $0.023\,e$ from the molecule to the SWCNT. This negligible charge transfer further supports the physisorption character of the interaction.

The initial plan was to analyze one representative configuration from each structural group in order to assess whether more extensive electronic structure analysis was necessary. Because the results for the global minimum configuration already indicated weak interaction and a physisorption mechanism, the analysis was not extended to all 14 unique local-minimum structures. Instead, representative structures from each structural group and subgroup were investigated, as introduced at the beginning of this section.

During the investigation, the HOMO distribution and overall orbital shapes were similar across the representative configurations from each structural group, with only minor variations observed in the location and extent of the overlapping states along the molecule. In contrast, a comparison of the LUMO visualizations between configurations revealed substantially larger differences, as shown in Figure 5.14.

As mentioned earlier in this section, for the representative structure of Group 1 (Structure ID 1), the honeycomb lattice pattern observed in the LUMO visualization was present only on the left side of the SWCNT, beneath the aromatic ring. In contrast, the right side of the SWCNT exhibited a more point-like electronic dis-

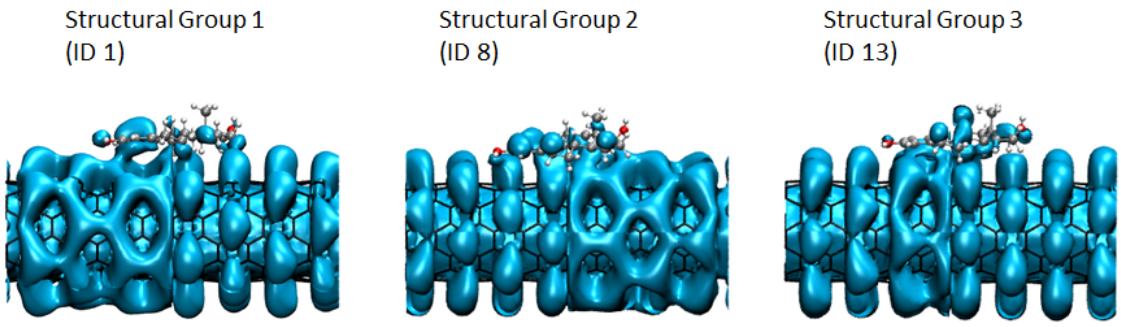

Figure 5.14: Visualization of the LUMO for representative adsorption configurations from each structural group (ID 1, ID 8, and ID 13) of E2 on a $(6, 6)$ SWCNT. The LUMO is plotted at an isosurface value of 0.001 e $Å^{-3}$.

tribution rather than a continuous honeycomb lattice structure. For Group 2, the representative structure (Structure ID 8) showed also a honeycomb lattice pattern only on part of the SWCNT surface rather than across the entire surface. Notably, the honeycomb lattice appeared on the side of the SWCNT that was not located beneath the aromatic ring of E2. Finally, in the Group 3 structure (Structure ID 13), only a small honeycomb lattice pattern was observed, localized directly beneath the aromatic ring of the molecule, while the rest of the SWCNT exhibited a more point-like electronic distribution. Compared to the representative structures of Groups 1 and 2, Group 3 differs mainly in the much smaller extent of the continuous honeycomb lattice pattern. In contrast, Groups 1 and 2 exhibit a similar partial honeycomb structure distributed over approximately half of the SWCNT surface, but on opposite sides.

6 Discussion

The objective of this thesis was first to address RQ1 through a review of the existing literature, which examined the ability of CNT-based electrochemical sensors to detect E2 in water samples. Based on the literature discussed in Chapter 2, CNT-based sensors have already been successfully investigated for E2 detection, with many studies employing functionalized CNT electrodes to improve sensitivity and selectivity. However, as discussed at the end of Chapter 2, a detailed understanding of adsorption on pristine SWCNTs at the atomic level remains limited and would be beneficial to establish before introducing functionalization. This motivated the subsequent objectives of this study, which were to identify the most stable adsorption configurations of E2 on a $(6, 6)$ SWCNT and to analyze the nature of the adsorption using computational simulations, with the aim of generating knowledge relevant for the development of electrochemical sensors for detecting contaminants in aquatic environments.

The structure search was carried out by employing a combination of the machine-learning-based BOSS algorithm and DFT to systematically sample the AES. As a result, 14 unique adsorption configurations were identified. These configurations differ mainly in the molecular orientation relative to the $(6, 6)$ SWCNT's long axis, the adsorption distance, and the adsorption site, defined by the position of the molecule's COM above the SWCNT surface.

The interaction between E2 and the $(6, 6)$ SWCNT is governed by physisorption. The obtained adsorption distances ($\approx$ 3.7–3.8 Å) are too large for covalent bond formation, which typically requires distances of $\sim$ 2 Å. This interpretation is supported by the electronic structure analysis: the pDOS contribution of E2 to the total DOS of the system is small and does not introduce new states near the Fermi level. In addition, the Mulliken charge analysis reveals only minimal charge transfer from the molecule to the SWCNT, which is consistent with weak vdW interactions. Typical vdW interaction strengths between individual atom pairs are on the order of 0.004–0.04 eV, although the total interaction energy can vary depending on the macroscopic geometry of the interacting substances. In this study, the calculated adsorption energy is approximately -0.77 eV. This relatively large adsorption energy compared to simple pairwise vdW interactions is physically reasonable, as the large size of the system allows the cumulative contribution of several tens of weak atom–atom interactions, together with π–π stacking between the aromatic ring of E2 and the $(6, 6)$ SWCNT surface, to produce an adsorption energy of this magnitude. A similar interpretation was reported by Sippola for E2 adsorption on graphene, where physisorption was likewise identified as the dominant interaction [12].

The identified physisorption is advantageous for sensing applications, because adsorption governed by physical interactions rather than covalent bonding enables reversible adsorption and desorption of target molecules. In physisorption, changes in the electronic properties arise primarily from variations in electron and hole carrier mobility rather than from significant charge transfer [101]. In addition, the LUMO visualization reveals that the hexagonal lattice pattern of the $(6, 6)$ SWCNT depends on the molecular adsorption configuration. In some structures, a more extended hexagonal pattern is observed over the external surface of the SWCNT, indicating the presence of multiple conductive pathways for electron transport. This may contribute to stable and reproducible signal generation. Nevertheless, the absence

of new electronic states near the Fermi level and the low Mulliken charge transfer indicate that adsorption has a minor effect on electronic structure. As a result, the sensor signal is likely to be sensitive to subtle environmental changes, because the adsorption causes only a small change in the electronic structure, which can be easily affected by external factors such as thermal fluctuations, solvent effects, or small changes in molecular orientation. While physisorption may enhance sensitivity, it can also make the response more susceptible to noise and less pronounced than in systems dominated by strong chemisorption.

Comparison of the present results with previous computational studies is limited, as only a few comparable studies are available and most are less exhaustive due to the high computational cost of adsorption structure searches. Typically, molecular locations on the surface are preselected based on chemical intuition, and different possible configurations examined by manually changing the molecular position or orientation rather than systematically.

Zaib et al. investigated the adsorption of E2 and BPA on SWCNTs and graphene using both experimental and computational approaches [10]. In their computational section, they employed an (18,0) SWCNT and DFT calculations using the B3LYP functional. The main difference from the present work lies in the configuration-search strategy: adsorption structures were generated by randomly placing the molecule on the surface with minimum molecule–surface distances ranging from 1.5 to 5 Å, resulting in more than 10 000 configurations, of which only the lowest-energy structures were analyzed in detail. In contrast, the BOSS-based approach used in this study required only approximately 1000 sampled configurations while still identifying the relevant low-energy structures, demonstrating substantially higher computational efficiency. The lowest-energy E2 configuration reported by Zaib et al. is structurally similar to the global minimum identified in this thesis: the methyl group points away from the $(6, 6)$ SWCNT surface, molecule is oriented more parallel than

perpendicular to the SWCNT's long axis. However, the orientation is described qualitatively, and no specific angle is reported, which limits direct quantitative comparison. They reported an adsorption energy of −26.2 kcal/mol (−1.14 eV), which is comparable in magnitude but somewhat stronger than the value obtained in this thesis. This stronger interaction may be attributed to the larger diameter and lower curvature of the $(18, 0)$ SWCNT compared to the $(6, 6)$ SWCNT, which enhances orbital overlap between E2 and the surface. This interpretation is supported by the reported adsorption energy of E2 on graphene −34.1 kcal/mol (−1.48 eV) in the Zaib et al. study. They concluded that adsorption is more favorable on graphene than on SWCNTs, as the planar geometry of graphene maximizes π–π interactions that are partially limited by SWCNT curvature. Although the nature of the adsorption on SWCNT was not explicitly classified in the Zaib et al. study, the reported adsorption energies and emphasis on π–π interactions suggest that the interaction is dominated by physisorption.

Similar types of interactions to those reported by Zaib et al. have also been identified for the adsorption of EE2 on SWCNTs [9] as well as for the adsorption of E2 on graphene oxide surfaces [15, 42]. These studies consistently indicate that the dominant interactions arise from noncovalent electrostatic contributions, particularly π–π interactions between the aromatic rings of the estrogen molecules and the carbon-based surfaces. Notably, de Oliveira et al. explicitly classified the adsorption of E2 on graphene oxide as physisorption driven by π–π interactions, based on both computational and experimental evidence [15].

The same computational workflow as presented in this thesis was also used in the study conducted by Sippola et al. [14], who investigated the adsorption of E2 on a pristine graphene sheet. Their calculations yielded two minimum-energy configurations and an adsorption energy of −1.56 eV, which is significantly larger than the −0.77 eV obtained in this thesis. Although this result further supports the

idea that adsorption strength increases as the curvature of the adsorbent decreases, the observed differences in adsorption energies may also arise from the different vdW correction schemes used in their study compared to those employed here. Different dispersion correction methods describe intermolecular interactions using distinct theoretical approximations, leading to variations in the predicted strength of molecule–surface interactions [85, 86]. The reported adsorption distance and the flattening of the molecular backbone compared to the gas-phase structure in the study by Sippola et al. are consistent with those reported here. They observed slightly larger adsorption distances for the minimum-energy structures (3.84 Å and 3.88 Å) compared to the values obtained in this study (3.72–3.80 Å). This difference may be attributed to the definition of the adsorption distance: in their work, the distance was measured from the lowest atom of graphene to the COM of E2, whereas in this study, it was defined between the SWCNT surface and the COM of E2. An indication of molecular backbone flattening, compared to the gas-phase structure, is the observed 1.1 Å lowering of the phenolic O atom at one end of the molecule. A similar, $\sim$0.5 Å lowering toward the surface, was observed in all identified configurations in this study. Notably, the possible shift in the overall height of the E2 molecule between the gas-phase and relaxed structures was not taken into account, which may partly explain the observed lowering of the phenolic O atom.

The combined computational workflow utilized in this thesis offers several advantages compared to simulations performed using DFT alone. The BOSS framework employs BO to determine the next sampling location, thereby reducing human bias while still enabling a thorough exploration of the AES to identify relevant adsorption configurations. This is evident when compared to the search strategy used in Zaib et al. [10]. To further reduce the computational cost, expert knowledge was used to define appropriate degrees of freedom and to apply symmetry constraints during the simulations. Due to the nature of the BOSS algorithm, the system struc-

ture was simplified with the use of building-block approach. As a result, internal structural changes of the molecule were captured only after the structure search, during the subsequent relaxation steps. The most notable change was the phenolic O atom moving closer to the surface, while other internal structural changes were not investigated in detail. In the case of E2, which is a relatively rigid molecule, this simplification is unlikely to have excluded important adsorption configurations. Therefore, the structure-search strategy is expected to capture the essential adsorption behavior without significant loss of information.

One remaining question concerns the impact of the applied symmetry function on the efficiency and quality of the structure search. Although symmetry constraints were introduced to reduce the search space and computational cost, the present results suggest that the underlying adsorption landscape may not strictly follow this assumed symmetry. A more thorough investigation of the symmetry properties of the system would therefore be necessary to confirm whether the applied symmetry constraints were fully justified. Another aspect related to the use of the symmetry function is that it effectively doubles the amount of generated data during simulations. For large and complex systems, it is therefore important to carefully consider whether the application of symmetry functions provides additional meaningful insight.

Despite their atomic-level insights, computational studies are not yet sufficient as standalone tools for sensor design because of the complex nature of sensing systems and their operating environments. As in this thesis, simulations are typically performed under vacuum conditions using highly simplified system designs. Such models cannot fully represent real-world environments. Important factors such as pH, temperature variations, solvation effects, and the presence of competing or interfering molecules are not included, even though they can significantly influence adsorption behavior. Without accounting for molecular interference, it is difficult

to draw firm conclusions about the selectivity of a given material toward a specific target molecule. These reasons highlight the need for studies that combine computational and experimental approaches, allowing simulation results to be validated and refined. Such integration is especially important in the context of water contamination, where detection systems must operate in chemically and environmentally complex conditions. Moreover, the effective use of the methods described in Chapter 3 requires careful selection of simulation parameters and a good understanding of the system being studied. While methods such as DFT are widely used and well established, their accurate application still depends on informed choices regarding model setup and interpretation of results.

As discussed, increasing human activities such as industrialization, urbanization, and climate change have intensified the contamination of limited clean water resources, making it a growing global concern. To ensure that water resources remain capable of sustaining life in the future, improved water monitoring strategies and more efficient purification technologies are urgently needed.

A clear example of the growing concern over water contamination can be seen in the United Nations Sustainable Development Goals (SDGs). Many of these goals are directly or indirectly linked to ensuring access to clean water, safeguarding aquatic environments, reducing exposure to toxic chemicals, and developing sustainable manufacturing practices that do not pose risks to humans or other living organisms [102, 103]. The level and sources of water contamination vary significantly by region. In developing countries, contamination is often primarily caused by insufficient wastewater treatment and inadequate sanitation systems, which are strongly linked to high child mortality rates. According to UNICEF's Triple Threat report [104], unsafe water, sanitation, and hygiene conditions result in approximately 1,000 child deaths per day. By contrast, in developed countries, major contributors include agricultural runoff and industrial discharges [105].

In situations where contaminated water sources are the only available option, the development of improved electrochemical sensors alone cannot fully resolve the problem, because knowledge of contamination does not eliminate exposure. Nevertheless, monitoring can generate data with broader societal impact. Such data collection is demonstrated in the study by Bain et al., conducted under the framework of the SDGs, which included large-scale efforts to monitor drinking water quality through nationally representative household surveys in low- and middle-income countries [106]. This type of monitoring enables the identification of risk factors and supports effective risk management and policy interventions. It can guide decision-making by identifying where treatment is most urgently needed, supporting the allocation of resources such as point-of-use treatment systems, and informing public health advisories. In addition, regular monitoring can function as an early warning system, enabling corrective actions such as boil-water notices or emergency chlorination and allowing short-lived contamination events, resulting from chemical leaks or flooding, to be detected before they cause widespread harm.

Achieving SDG targets, however, requires actions beyond monitoring. UNICEF has estimated that investments of approximately US$114 billion per year are needed to meet goals in developing regions [104]. This highlights the need for increased investment in green technologies, resilient sanitation infrastructure, and water purification systems that can withstand climate-related stresses. In the short term, locally adapted and low-cost solutions, such as simple filtration methods and the use of contaminated water for non-potable purposes, can help reduce exposure risks some time, but in a long term, sustained investment in infrastructure, governance, and policy is essential to manage and protect water resources.

In developed countries, the focus is often on regulating industrial and agricultural emissions and the use of chemicals, such as pesticides and pharmaceuticals. Accurate monitoring is essential for identifying which substances enter the environ-

ment through runoff and determining their potential ecological and health impacts. Reliable data are also necessary for establishing exposure limits that do not pose risks to humans or wildlife, and for ensuring compliance with existing regulations through continuous surveillance. For these reasons, electrochemical sensors provide several advantages over conventional chromatographic methods. Sensors are more easily mass-produced, can be designed for on-site and real-time monitoring, and allow rapid response to contamination events. Moreover, because sensor performance is strongly influenced by electrode materials, electrochemical sensors can be iteratively improved and optimized through a combination of experimental testing and modeling, making them a flexible and scalable solution for addressing current and future water quality challenges.

Beyond environmental applications, electrochemical sensors have also attracted significant interest in the medical field for diagnostic and health-monitoring purposes. With the growing trend toward continuous and personalized health monitoring, sensor-based technologies offer promising solutions for reducing the burden on healthcare systems and hospital capacity. In medical research and clinical practice, accurate monitoring of compounds such as neurotransmitters and hormones in the human body is crucial for understanding physiological processes and disease progression. However, many conventional analytical methods remain limited in their ability to provide efficient and reliable biological monitoring. They are often costly, time-consuming, and resource-intensive, while also lacking sufficient temporal and spatial resolution to capture dynamic biological processes. Furthermore, their practical application is hindered by challenges related to selectivity, as structurally similar compounds may interfere with target detection. In addition, for in vivo applications, sensors must meet strict requirements for biocompatibility and minimal toxicity, which are not always satisfied by electrodes based on metal oxides. In this context, electrochemical sensors with carbon-based electrodes represent a

promising alternative, as they offer high sensitivity, selectivity, real-time monitoring capabilities, and good biocompatibility. These advantages highlight their potential for reliable biomedical monitoring and further emphasize the broader relevance of sensing mechanisms investigated in this work.

To better connect these sensing applications with the atomistic insights obtained in this work, a natural next step is to investigate how adsorption influences the electronic transport properties of SWCNTs, such as electrical conductivity. Such analyses are particularly relevant when assessing the suitability of a surface material for electrochemical sensors, as changes in conductivity directly influence sensor response. Transport properties can be investigated, for example, using Boltzmann transport calculations [107], which provide a framework for describing charge transport in systems driven out of equilibrium. Adsorption can change the electronic structure of a SWCNT, thereby modifying charge carrier transport along the surface. Because SWCNTs exhibit different electronic characteristics depending on their chirality, the impact of adsorption on conductivity may vary significantly between different SWCNT types. Therefore, combining adsorption studies with Boltzmann transport calculations would enable the establishment of a more direct link between molecular adsorption and sensor signal generation.

In addition to investigating transport properties during adsorption, future studies could be extended to examine different SWCNT chiralities in order to determine whether chirality influences adsorption behavior and whether certain chiralities exhibit enhanced selectivity toward specific molecules, as suggested by the experimental study of Seo et al. about dopamine adsorption on (6,6) and (6,5) SWCNTs [77]. An important question is whether adsorption strength increases primarily with SWCNT diameter or whether chirality itself is the dominant factor governing these interactions. Furthermore, future simulations should more accurately account for environmental parameters by incorporating solvent models that represent aqueous conditions. Including solvation effects would provide insight into how adsorption behavior changes in realistic water matrices.

7 Conclusions

In this thesis, the adsorption of 17β-estradiol on a $(6, 6)$ single-walled carbon nanotube was investigated computationally. Adsorption simulations were conducted using the Bayesian Optimization Structure Search algorithm, and the resulting configurations were analyzed in terms of their electronic structure, energetics, and structural properties. The aim was to gain atomistic insight into the adsorption mechanisms governing the interaction between E2 and $(6, 6)$ SWCNT surfaces, with relevance to electrochemical sensor development.

This computational study was placed in a broader context through a literature review of current detection methods for EDCs, including E2, in water samples. Exposure to EDCs poses significant risks to aquatic ecosystems and human health, even at very low concentrations, and their effects may only become apparent after long-term exposure. Current gold-standard analytical techniques, such as chromatographic methods, provide high sensitivity but suffer from limitations related to cost, complexity, and lack of suitability for in situ and real-time monitoring. These challenges have increased interest in electrochemical sensors as alternative monitoring tools.

Based on the results of this thesis, the research questions posed at the beginning can be addressed as follows:

RQ1: What does the existing literature indicate about the ability of carbon nanotube-based electrochemical sensors to detect 17β-estradiol

(E2) in water samples? Based on the literature review, CNT-based materials have been shown to be effective for detecting E2 in water samples, with several studies reporting successful detection using functionalized electrochemical sensors, where functionalization is employed to enhance sensor selectivity. However, understanding the intrinsic adsorption behavior of pristine SWCNTs is essential for evaluating the role of chirality and identifying SWCNT structures that may not require additional modification. This study suggests that further investigation of different SWCNT chiralities and environmental effects is needed to determine whether pristine SWCNTs can achieve sufficient selectivity under realistic conditions. At present, CNT–based sensing appears promising, but optimization strategies and application-specific designs are still required, particularly to achieve reliable performance under realistic concentration levels.

RQ2: What are the most stable and energetically favorable adsorption configurations of 17β-estradiol on a $(6, 6)$ **SWCNT surface?** In the computational part of this thesis, 14 unique adsorption configurations of E2 on a $(6, 6)$ SWCNT were identified. These configurations were divided into three structural groups based on geometric metrics defined in this study. Most adsorption configurations shared similar structural characteristics, indicating relatively uniform adsorption behavior. The adsorption energies ranged from -0.77 to -0.74 eV, while the adsorption distances varied between 3.71 and 3.80 Å. A correlation between adsorption energy and distance was observed, with lower-energy configurations generally corresponding to shorter adsorption distances. The molecular orientation relative to the SWCNT long axis showed the largest variation between configurations, with the most favorable orientation angle being approximately 18°. A few structures were nearly aligned with the SWCNT long axis, corresponding to orientation angles of around 4°.

RQ3: What types of interactions occur between E2 and a (6,6) SWCNT, and are any covalent bonds formed? Electronic structure analysis indicates that E2 adsorption on the $(6, 6)$ SWCNT is governed by physisorption dominated by vdW interactions. The adsorption distances are too large to support covalent bond formation, and Mulliken charge analysis revealed only minimal charge transfer between the molecule and the SWCNT. Additionally, DOS calculations showed no new states or significant peak shifts upon adsorption. The DOS exhibited only well-defined, sharp individual peaks, which are characteristic of physisorption, while broader and lower peaks associated with orbital hybridization, which are typical of chemisorption, were not observed. The calculated adsorption energies are relatively weak (above -0.8 eV), further supporting the physisorption mechanism. Additionally, the presence of multiple adsorption configurations within approximately 25 meV of the global minimum suggests that, at room temperature, E2 molecules may diffuse across the $(6, 6)$ SWCNT surface rather than remain fixed at a single adsorption site. Consequently, multiple configurations may coexist dynamically under realistic conditions.

Overall, this thesis demonstrates that adsorption-based electrochemical sensors offer a portable and scalable alternative to conventional analytical techniques for monitoring EDCs in water samples. Although this work represents an initial step, it highlights several promising directions for future research, including examining the effects of adsorption on the electrical transport properties of SWCNTs (e.g., conductivity), performing systematic investigations of SWCNT chirality, incorporating environmental factors such as solvation effects, temperature, and pH changes into simulations, and integrating sensing platforms with water purification systems.

Furthermore, this work highlights how computational approaches, combined with machine learning methods such as the BOSS, enable more efficient exploration of complex adsorption landscapes. The integration of computational and experimen-

tal studies can accelerate sensor development and improve performance. Continued methodological advancements are required to better account for environmental conditions and bridge the gap between simulations and real world systems. Improved water quality monitoring supports better regulation and legislation, ultimately guiding industries and governments toward more sustainable practices. In this way, advances in electrochemical sensing and computational modeling contribute to safeguarding water resources and protecting future generations.

References

[1] W. Musie and G. Gonfa, "Fresh water resource, scarcity, water salinity challenges and possible remedies: A review", *Heliyon*, vol. 9, no. 8, pp. 1–18, 2023. DOI: 10.1016/j.heliyon.2023.e18685.

[2] E. N. Hilz and A. C. Gore, "Endocrine-Disrupting Chemicals: Science and Policy", *Policy Insights from the Behavioral and Brain Sciences*, vol. 10, no. 2, pp. 142–150, 2023. DOI: 10.1177/23727322231196794.

[3] Y. Combarnous and T. M. D. Nguyen, "Comparative Overview of the Mechanisms of Action of Hormones and Endocrine Disruptor Compounds", *Toxics*, vol. 7, no. 1, p. 5, 2019. DOI: 10.3390/toxics7010005.

[4] L. Wang, H. Wang, C. Tizaoui, Y. Yang, J. Ali, and W. Zhang, "Endocrine disrupting chemicals in water and recent advances on their detection using electrochemical biosensors", *Sensors & Diagnostics*, vol. 2, no. 1, pp. 46–77, 2023. DOI: 10.1039/D2SD00156J.

[5] A. C. Gore, L. M. Thompson, M. Bell, and J. A. Mennigen, "Transgenerational effects of polychlorinated biphenyls: 2. Hypothalamic gene expression in rats", *Biology of Reproduction*, vol. 105, no. 3, pp. 690–704, 2021. DOI: 10.1093/biolre/ioab066.

[6] M. Adeel, X. Song, Y. Wang, D. Francis, and Y. Yang, "Environmental impact of estrogens on human, animal and plant life: A critical review", *Environment*

International, vol. 99, pp. 107–119, 2017. DOI: 10.1016/j.envint.2016.12.010.

[7] E. Simon et al., "Biological effect and chemical monitoring of Watch List substances in European surface waters: Steroidal estrogens and diclofenac – Effect-based methods for monitoring frameworks", *Environment International*, vol. 159, p. 107 033, 2022. DOI: 10.1016/j.envint.2021.107033.

[8] T. F. T. Omar, A. Ahmad, A. Z. Aris, and F. M. Yusoff, "Endocrine disrupting compounds (EDCs) in environmental matrices: Review of analytical strategies for pharmaceuticals, estrogenic hormones, and alkylphenol compounds", *TrAC Trends in Analytical Chemistry*, vol. 85, pp. 241–259, 2016. DOI: 10.1016/j.trac.2016.08.004.

[9] L. Joseph, J. Heo, Y.-G. Park, J. R. V. Flora, and Y. Yoon, "Adsorption of bisphenol A and 17α-ethinyl estradiol on single walled carbon nanotubes from seawater and brackish water", *Desalination*, vol. 281, pp. 68–74, 2011. DOI: 10.1016/j.desal.2011.07.044.

[10] Q. Zaib, I. A. Khan, N. B. Saleh, J. R. V. Flora, Y.-G. Park, and Y. Yoon, "Removal of Bisphenol A and 17β-Estradiol by Single-Walled Carbon Nanotubes in Aqueous Solution: Adsorption and Molecular Modeling", *Water, Air, & Soil Pollution*, vol. 223, no. 6, pp. 3281–3293, 2012. DOI: 10.1007/s11270-012-1109-5.

[11] J. Järvi, B. Alldritt, O. Krejčí, M. Todorović, P. Liljeroth, and P. Rinke, "Integrating Bayesian Inference with Scanning Probe Experiments for Robust Identification of Surface Adsorbate Configurations", *Advanced Functional Materials*, vol. 31, no. 32, pp. 1–8, 2021. DOI: 10.1002/adfm.202010853.

[12] S. Sippola, *Adsorption of 17-β(beta)-estradiol on pristine graphene: A first-principles sructure search study*, Master's thesis, Aalto University, 2024. [Online]. Available: https://urn.fi/URN:NBN:fi:aalto-202411217348.

[13] M. Todorović, M. U. Gutmann, J. Corander, and P. Rinke, "Bayesian inference of atomistic structure in functional materials", *npj Computational Materials*, vol. 5, no. 1, p. 35, 2019. DOI: 10.1038/s41524-019-0175-2.

[14] S. Sippola, M. Todorović, and E. Peltola, "First-Principles Structure Search Study of 17β-Estradiol Adsorption on Graphene", *ACS Omega*, vol. 9, no. 32, pp. 34 684–34 691, 2024. DOI: 10.1021/acsomega.4c03485.

[15] P. V. de Oliveira, I. Zanella, L. O. S. Bulhões, and S. B. Fagan, "Adsorption of 17β-Estradiol in graphene oxide through the competing methanol co-solvent: Experimental and computational analysis", *Journal of Molecular Liquids*, vol. 321, p. 114 738, 2021. DOI: 10.1016/j.molliq.2020.114738.

[16] V. Singh, R. K. Srivastava, and A. K. Bhatt, "Sources of water pollution", in *Battling Air and Water Pollution: Protecting Our Planet's Vital Resources*. Singapore: Springer Nature, 2025, pp. 97–110. DOI: 10.1007/978-981-96-4375-2_7.

[17] B. N. Khan et al., "Elucidating the effects of heavy metals contamination on vital organ of fish and migratory birds found at fresh water ecosystem", *Heliyon*, vol. 9, no. 11, pp. 1–15, 2023. DOI: 10.1016/j.heliyon.2023.e20968.

[18] O. M. Rodriguez-Narvaez, J. M. Peralta-Hernandez, A. Goonetilleke, and E. R. Bandala, "Treatment technologies for emerging contaminants in water: A review", *Chemical Engineering Journal*, vol. 323, pp. 361–380, 2017. DOI: 10.1016/j.cej.2017.04.106.

[19] L. N. Vandenberg et al., "Hormones and Endocrine-Disrupting Chemicals: Low-Dose Effects and Nonmonotonic Dose Responses", *Endocrine Reviews*, vol. 33, no. 3, pp. 378–455, 2012. DOI: 10.1210/er.2011-1050.

[20] A. C. Gore et al., "EDC-2: The Endocrine Society's Second Scientific Statement on Endocrine-Disrupting Chemicals", *Endocrine Reviews*, vol. 36, no. 6, E1–E150, 2015. DOI: 10.1210/er.2015-1010.

[21] K. Mattonet et al., "Prenatal exposure to endocrine disrupting chemicals is associated with altered DNA methylation in cord blood", *Epigenetics*, vol. 17, no. 9, pp. 935–952, 2021. DOI: 10.1080/15592294.2021.1975917.

[22] A. Alavian-Ghavanini et al., "Prenatal Bisphenol A Exposure is Linked to Epigenetic Changes in Glutamate Receptor Subunit Gene Grin2b in Female Rats and Humans", *Scientific Reports*, vol. 8, no. 1, p. 11 315, 2018. DOI: 10.1038/s41598-018-29732-9.

[23] C. Duh-Leong, M. V. Maffini, C. D. Kassotis, L. N. Vandenberg, and L. Trasande, "The regulation of endocrine-disrupting chemicals to minimize their impact on health", *Nature Reviews Endocrinology*, vol. 19, no. 10, pp. 600–614, 2023. DOI: 10.1038/s41574-023-00872-x.

[24] European Commission, *Reach regulation*. Accessed: Sep. 16, 2025. [Online]. Available: https://environment.ec.europa.eu/topics/chemicals/reach-regulation_en.

[25] European Commission, *Water framework directive*. Accessed: Nov. 30, 2025. [Online]. Available: https://environment.ec.europa.eu/topics/water/water-framework-directive_en.

[26] M. Bilal, D. Barceló, and H. M. N. Iqbal, "Occurrence, environmental fate, ecological issues, and redefining of endocrine disruptive estrogens in water

resources", *Science of The Total Environment*, vol. 800, p. 149 635, 2021. DOI: 10.1016/j.scitotenv.2021.149635.

[27] P. P. Waifalkar, D. Noh, P. Derashri, S. Barage, and E. Oh, "Role of Estradiol Hormone in Human Life and Electrochemical Aptasensing of 17β-Estradiol: A Review", *Biosensors*, vol. 12, no. 12, p. 1117, 2022. DOI: 10.3390/bios12121117.

[28] H. Tapiero, G. Nguyen Ba, and K. D. Tew, "Estrogens and environmental estrogens", *Biomedicine & Pharmacotherapy*, vol. 56, no. 1, pp. 36–44, 2002. DOI: 10.1016/S0753-3322(01)00155-X.

[29] R. S. Vardanyan and V. J. Hruby, "28 - female sex hormones", in *Synthesis of Essential Drugs*, R. S. Vardanyan and V. J. Hruby, Eds. Amsterdam: Elsevier, 2006, pp. 365–379. DOI: 10.1016/B978-044452166-8/50028-5.

[30] F. Z. Stanczyk, "Metabolism of endogenous and exogenous estrogens in women", *The Journal of Steroid Biochemistry and Molecular Biology*, vol. 242, p. 106 539, 2024. DOI: 10.1016/j.jsbmb.2024.106539.

[31] A. Glineur, K. Nott, P. Carbonnelle, S. Ronkart, T. Pollet, and G. Purcaro, "Occurrence and environmental risk assessment of 4 estrogenic compounds in surface water in Belgium in the frame of the EU Watch List", *Environmental Science and Pollution Research*, vol. 31, no. 5, pp. 6857–6873, 2023. DOI: 10.1007/s11356-023-31698-9.

[32] F. Fruzzetti, T. Fidecicchi, M. M. Montt Guevara, and T. Simoncini, "Estetrol: A New Choice for Contraception", *Journal of Clinical Medicine*, vol. 10, no. 23, p. 5625, 2021. DOI: 10.3390/jcm10235625.

[33] N. Leroux et al., "Assessment of the effects of estetrol and 17α-ethinylestradiol on zebrafish (*Danio rerio*) metamorphosis: A morphological

and transcriptomic approach", *Environmental Pollution*, vol. 376, p. 126 423, 2025. DOI: 10.1016/j.envpol.2025.126423.

[34] G.-G. Ying, R. S. Kookana, and Y.-J. Ru, "Occurrence and fate of hormone steroids in the environment", *Environment International*, vol. 28, no. 6, pp. 545–551, 2002. DOI: 10.1016/S0160-4120(02)00075-2.

[35] P. B. Hamilton et al., "Feminizing effects of ethinylestradiol in roach (Rutilus rutilus) populations with different estrogenic pollution exposure histories", *Aquatic Toxicology (Amsterdam, Netherlands)*, vol. 249, p. 106 229, 2022. DOI: 10.1016/j.aquatox.2022.106229.

[36] K. A. Kidd et al., "Collapse of a fish population after exposure to a synthetic estrogen", *Proceedings of the National Academy of Sciences*, vol. 104, no. 21, pp. 8897–8901, 2007. DOI: 10.1073/pnas.0609568104.

[37] L. Jackson and P. Klerks, "Effects of the synthetic estrogen 17α-ethinylestradiol on Heterandria formosa populations: Does matrotrophy circumvent population collapse?", *Aquatic Toxicology (Amsterdam, Netherlands)*, vol. 229, p. 105 659, 2020. DOI: 10.1016/j.aquatox.2020.105659.

[38] Y. Lu et al., "Neuron-Derived Estrogen Regulates Synaptic Plasticity and Memory", *The Journal of Neuroscience*, vol. 39, no. 15, pp. 2792–2809, 2019. DOI: 10.1523/JNEUROSCI.1970-18.2019.

[39] L. R. Taxier, K. S. Gross, and K. M. Frick, "Oestradiol as a neuromodulator of learning and memory", *Nature Reviews Neuroscience*, vol. 21, no. 10, pp. 535–550, 2020. DOI: 10.1038/s41583-020-0362-7.

[40] F. Z. Stanczyk and N. J. Clarke, "Measurement of estradiol–challenges ahead", *The Journal of Clinical Endocrinology and Metabolism*, vol. 99, no. 1, pp. 56–58, 2014. DOI: 10.1210/jc.2013-2905.

[41] S. Zinn and M. Schnell, "Flexibility at the Fringes: Conformations of the Steroid Hormone β-Estradiol", *ChemPhysChem*, vol. 19, no. 21, pp. 2915–2920, 2018. DOI: 10.1002/cphc.201800647.

[42] P. Borthakur, P. K. Boruah, M. R. Das, N. Kulik, and B. Minofar, "Adsorption of 17α-ethynyl estradiol and β-estradiol on graphene oxide surface: An experimental and computational study", *Journal of Molecular Liquids*, vol. 269, pp. 160–168, 2018. DOI: 10.1016/j.molliq.2018.08.013.

[43] F. Fruzzetti and J. Bitzer, "Review of clinical experience with estradiol in combined oral contraceptives", *Contraception*, vol. 81, no. 1, pp. 8–15, 2010. DOI: 10.1016/j.contraception.2009.08.010.

[44] S. D'Arpe, M. D. Feliciantonio, M. Candelieri, S. Franceschetti, M. G. Piccioni, and C. Bastianelli, "Ovarian function during hormonal contraception assessed by endocrine and sonographic markers: A systematic review", *Reproductive BioMedicine Online*, vol. 33, no. 4, pp. 436–448, 2016. DOI: 10.1016/j.rbmo.2016.07.010.

[45] P. Bjerregaard, P. R. Hansen, K. J. Larsen, C. Erratico, B. Korsgaard, and H. Holbech, "Vitellogenin as a biomarker for estrogenic effects in brown trout, Salmo trutta: Laboratory and field investigations", *Environmental Toxicology and Chemistry*, vol. 27, no. 11, pp. 2387–2396, 2008. DOI: 10.1897/08-148.1.

[46] M. Woods and A. Kumar, "Vitellogenin induction by 17β-estradiol and 17α-ethynylestradiol in male Murray rainbowfish (Melanotaenia fluviatilis)", *Environmental Toxicology and Chemistry*, vol. 30, no. 11, pp. 2620–2627, 2011. DOI: 10.1002/etc.660.

[47] O. Coskun, "Separation techniques: Chromatography", *Northern Clinics of Istanbul*, vol. 3, no. 2, pp. 156–160, 2016. DOI: 10.14744/nci.2016.32757.

[48] A. Glineur, K. Nott, P. Carbonnelle, S. Ronkart, and G. Purcaro, "Development And Validation Of A Method For Determining Estrogenic Compounds In Surface Water At The Ultra-Trace Level Required By The EU Water Framework Directive Watch List", *Journal of Chromatography A*, vol. 1624, p. 461 242, 2020. DOI: 10.1016/j.chroma.2020.461242.

[49] R. Elfadul, R. Jesien, A. Elnabawi, P. Chigbu, and A. Ishaque, "Analysis of Estrogenic Activity in Maryland Coastal Bays Using the MCF-7 Cell Proliferation Assay", *International Journal of Environmental Research and Public Health*, vol. 18, no. 12, p. 6254, 2021. DOI: 10.3390/ijerph18126254.

[50] S. Fouyet, M.-C. Ferger, P. Leproux, P. Rat, and M. Dutot, "Advancing Endocrine Disruptors via In Vitro Evaluation: Recognizing the Significance of the Organization for Economic Co-Operation and Development and United States Environmental Protection Agency Guidelines, Embracing New Assessment Methods, and the Urgent Need for a Comprehensive Battery of Tests", *Toxics*, vol. 12, no. 3, p. 183, 2024. DOI: 10.3390/toxics12030183.

[51] W. Xia et al., "Electrochemical biosensor for estrogenic substance using lipid bilayers modified by Au nanoparticles", *Biosensors and Bioelectronics*, vol. 25, no. 10, pp. 2253–2258, 2010. DOI: 10.1016/j.bios.2010.03.004.

[52] D. Tu, J. T. Garza, and G. L. Coté, "A SERS aptasensor for sensitive and selective detection of bis(2-ethylhexyl)phthalate", *RSC Advances*, vol. 9, no. 5, pp. 2618–2625, 2019. DOI: 10.1039/C8RA09230C.

[53] L. Zhang et al., "Electrochemical biosensors represent promising detection tools in medical field", *Advanced Sensor and Energy Materials*, vol. 2, no. 4, p. 100 081, 2023. DOI: 10.1016/j.asems.2023.100081.

[54] J. Lin, Y. Chen, X. Liu, H. Jiang, and X. Wang, "Engineered Intelligent Electrochemical Biosensors for Portable Point-of-Care Diagnostics", *Chemosensors*, vol. 13, no. 4, 2025. DOI: 10.3390/chemosensors13040146.

[55] A. Piras, C. Ehlert, and G. Gryn'ova, "Sensing and sensitivity: Computational chemistry of graphene-based sensors", *WIREs Computational Molecular Science*, vol. 11, no. 5, e1526, 2021. DOI: 10.1002/wcms.1526.

[56] M. Laurila, *Laskennallisten menetelmien soveltaminen hiilinanoputkipohjaisten sähkökemiallisten dopamiiniantureiden kehittämisessä*, Bachelor's thesis, University of Turku, 2025. [Online]. Available: https://urn.fi/URN:NBN:fi-fe202501204695.

[57] F. C. Moraes, B. Rossi, M. C. Donatoni, K. T. de Oliveira, and E. C. Pereira, "Sensitive determination of 17β-estradiol in river water using a graphene based electrochemical sensor", *Analytica Chimica Acta*, vol. 881, pp. 37–43, 2015. DOI: 10.1016/j.aca.2015.04.043.

[58] M. Ciślak, I. Kruszelnicka, J. Zembrzuska, and D. Ginter-Kramarczyk, "Estrogen pollution of the European aquatic environment: A critical review", *Water Research*, vol. 229, p. 119 413, 2023. DOI: 10.1016/j.watres.2022.119413.

[59] D. N. d. Silva and A. C. Pereira, "An electrochemical sensor modified with a molecularly imprinted polymer and carbon black for 17β-estradiol detection", *Analytical Methods*, vol. 14, no. 12, pp. 1208–1213, 2022. DOI: 10.1039/D1AY02062E.

[60] M. E. Weese-Myers and A. E. Ross, "Electrochemical characterization of 17β-estradiol with fast-scan cyclic voltammetry", *Electroanalysis*, vol. 35, no. 9, e202200560, 2023. DOI: 10.1002/elan.202200560.

[61] Y.-n. Zhang, Q. Niu, X. Gu, N. Yang, and G. Zhao, "Recent progress on carbon nanomaterials for the electrochemical detection and removal of environmental pollutants", *Nanoscale*, vol. 11, no. 25, pp. 11 992–12 014, 2019. DOI: 10.1039/C9NR02935D.

[62] V. Karthik et al., "Recent advances in electrochemical sensor developments for detecting emerging pollutant in water environment", *Chemosphere*, vol. 304, p. 135 331, 2022. DOI: 10.1016/j.chemosphere.2022.135331.

[63] International Union of Pure and Applied Chemistry (IUPAC), *Adsorption*, 2025. DOI: 10.1351/goldbook.A00155.

[64] O. D. Agboola and N. U. Benson, "Physisorption and Chemisorption Mechanisms Influencing Micro (Nano) Plastics-Organic Chemical Contaminants Interactions: A Review", *Frontiers in Environmental Science*, vol. 9, 2021. DOI: 10.3389/fenvs.2021.678574.

[65] G. Barnes and I. Gentle, *Interfacial Science: An Introduction*. Oxford University Press, 2023, pp. 43–56. DOI: 10.1093/hesc/9780199571185.001.0001.

[66] A. N. Raditya and D. O'Hare, "Review—Electrochemical Sensor Biofouling in Environmental Sensor Networks: Characterisation, Remediation and Lessons from Biomedical Devices", *Journal of The Electrochemical Society*, vol. 167, no. 12, p. 127 503, 2020. DOI: 10.1149/1945-7111/aba931.

[67] A. Karton, "π–π interactions between benzene and graphene by means of large-scale DFT-D4 calculations", *Chemical Physics*, vol. 561, p. 111 606, 2022. DOI: 10.1016/j.chemphys.2022.111606.

[68] B. Pan and B. Xing, "Adsorption mechanisms of organic chemicals on carbon nanotubes", *Environmental Science & Technology*, vol. 42, no. 24, pp. 9005–9013, 2008. DOI: 10.1021/es801777n.

[69] N. Gupta, S. M. Gupta, and S. K. Sharma, "Carbon nanotubes: Synthesis, properties and engineering applications", *Carbon Letters*, vol. 29, no. 5, pp. 419–447, 2019. DOI: 10.1007/s42823-019-00068-2.

[70] M. F. Budyka, T. S. Zyubina, A. G. Ryabenko, S. H. Lin, and A. M. Mebel, "Bond lengths and diameters of armchair single wall carbon nanotubes", *Chemical Physics Letters*, vol. 407, no. 4, pp. 266–271, 2005. DOI: 10.1016/j.cplett.2005.03.088.

[71] C.-H. Yeh, Y.-J. Hsiao, and J.-C. Jiang, "Dopamine sensing by boron and nitrogen co-doped single-walled carbon nanotubes: A first-principles study", *Applied Surface Science*, vol. 473, pp. 59–64, 2019. DOI: 10.1016/j.apsusc.2018.12.137.

[72] M. D. Esrafili, "Nitrogen-doped (6,0) carbon nanotubes: A comparative DFT study based on surface reactivity descriptors", *Computational and Theoretical Chemistry*, vol. 1015, pp. 1–7, 2013. DOI: 10.1016/j.comptc.2013.04.003.

[73] M. Baratta, A. V. Nezhdanov, A. I. Mashin, F. P. Nicoletta, and G. De Filpo, "Carbon nanotubes buckypapers: A new frontier in wastewater treatment technology", *Science of The Total Environment*, vol. 924, p. 171 578, 2024. DOI: 10.1016/j.scitotenv.2024.171578.

[74] G. Cho, S. Azzouzi, G. Zucchi, and B. Lebental, "Electrical and Electrochemical Sensors Based on Carbon Nanotubes for the Monitoring of Chemicals in Water—A Review", *Sensors*, vol. 22, no. 1, p. 218, Jan. 2022. DOI: 10.3390/s22010218. Accessed: Jan. 15, 2026.

[75] M. E. Wilson, M. G. Rukh, and M. A. Ashraf, "The role of nanotechnology, based on carbon nanotubes in water and wastewater treatment", *Desalination and Water Treatment*, vol. 242, pp. 12–21, 2021. DOI: 10.5004/dwt.2021.27568.

[76] Q. Guo, X.-t. Shen, Y.-y. Li, and S.-q. Xu, "Carbon nanotubes-based drug delivery to cancer and brain", *Current Medical Science*, vol. 37, no. 5, pp. 635–641, 2017. DOI: 10.1007/s11596-017-1783-z.

[77] J.-Y. Seo et al., "Single-chirality single-wall carbon nanotubes for electrochemical biosensing", *Physical Chemistry Chemical Physics*, vol. 27, no. 9, pp. 4959–4967, 2025. DOI: 10.1039/D4CP04206A.

[78] N. N. Nyangiwe, "The role of computational materials science in achieving sustainable development goals: A review", *Next Research*, vol. 2, no. 3, p. 100 692, 2025. DOI: 10.1016/j.nexres.2025.100692.

[79] J. Järvi, P. Rinke, and M. Todorović, "Detecting stable adsorbates of (1 *S*)-camphor on Cu(111) with Bayesian optimization", *Beilstein Journal of Nanotechnology*, vol. 11, pp. 1577–1589, 2020. DOI: 10.3762/bjnano.11.140.

[80] T. Tsuneda, *Density Functional Theory in Quantum Chemistry*. Tokyo: Springer Japan, 2014, pp. 1–124. DOI: 10.1007/978-4-431-54825-6.

[81] D. S. Sholl and J. A. Steckel, "What is density functional theory?", in *Density Functional Theory*. John Wiley Sons, Ltd, 2009, ch. 1, pp. 1–33. DOI: 10.1002/9780470447710.

[82] D. Rappoport, N. R. M. Crawford, F. Furche, and K. Burke, "Approximate Density Functionals: Which Should I Choose?", in *Encyclopedia of Inorganic Chemistry*. John Wiley & Sons, Ltd, 2009. DOI: 10.1002/0470862106.ia615.

[83] M. Bursch, J.-M. Mewes, A. Hansen, and S. Grimme, "Best-Practice DFT Protocols for Basic Molecular Computational Chemistry", *Angewandte Chemie*, vol. 134, no. 42, e202205735, 2022. DOI: 10.1002/ange.202205735.

[84] J. P. Perdew, K. Burke, and M. Ernzerhof, "Generalized Gradient Approximation Made Simple", *Physical Review Letters*, vol. 77, no. 18, pp. 3865–3868, 1996. DOI: 10.1103/PhysRevLett.77.3865.

[85] A. Tkatchenko, R. A. DiStasio, R. Car, and M. Scheffler, "Accurate and Efficient Method for Many-Body van der Waals Interactions", *Physical Review Letters*, vol. 108, no. 23, p. 236 402, 2012. DOI: 10.1103/PhysRevLett.108.236402.

[86] A. Ambrosetti, A. M. Reilly, R. A. DiStasio Jr., and A. Tkatchenko, "Long-range correlation energy calculated from coupled atomic response functions", *The Journal of Chemical Physics*, vol. 140, no. 18, 18A508, 2014. DOI: 10.1063/1.4865104.

[87] L. Fang, X. Guo, M. Todorović, P. Rinke, and X. Chen, "Exploring the Conformers of an Organic Molecule on a Metal Cluster with Bayesian Optimization", *Journal of Chemical Information and Modeling*, vol. 63, no. 3, pp. 745–752, 2023. DOI: 10.1021/acs.jcim.2c01120.

[88] M. Vaganova, I. Nesterova, Y. Kanygin, A. Kazennov, and A. Khlyupin, "Linking theoretical and simulation approaches to study fluids in nanoporous media: Molecular dynamics and classical density functional theory", *Chemical Engineering Science*, vol. 250, p. 117 383, 2022. DOI: 10.1016/j.ces.2021.117383.

[89] R. S. Mulliken, "Electronic Population Analysis on LCAO–MO Molecular Wave Functions. I", *The Journal of Chemical Physics*, vol. 23, no. 10, pp. 1833–1840, 1955. DOI: 10.1063/1.1740588.

[90] E. Runge, "Density-Functional Theory for Time-Dependent Systems", *Physical Review Letters*, vol. 52, no. 12, pp. 997–1000, 1984. DOI: 10.1103/PhysRevLett.52.997.

[91] S. Kiyohara, H. Oda, K. Tsuda, and T. Mizoguchi, "Acceleration of stable interface structure searching using a kriging approach", *Japanese Journal of Applied Physics*, no. 4, p. 045 502, 2016. DOI: 10.7567/JJAP.55.045502.

[92] Y. Wang, J. Lv, L. Zhu, and Y. Ma, "CALYPSO: A method for crystal structure prediction", *Computer Physics Communications*, vol. 183, no. 10, pp. 2063–2070, 2012. DOI: 10.1016/j.cpc.2012.05.008.

[93] J. Behler, "Representing potential energy surfaces by high-dimensional neural network potentials", *Journal of Physics: Condensed Matter*, vol. 26, no. 18, p. 183 001, 2014. DOI: 10.1088/0953-8984/26/18/183001.

[94] X. Wang, Y. Jin, S. Schmitt, and M. Olhofer, "Recent Advances in Bayesian Optimization", *ACM Comput. Surv.*, vol. 55, no. 13s, pp. 1–36, 2023. DOI: 10.1145/3582078.

[95] E. Brochu, V. M. Cora, and N. d. Freitas, *A Tutorial on Bayesian Optimization of Expensive Cost Functions, with Application to Active User Modeling and Hierarchical Reinforcement Learning*, 2010. DOI: 10.48550/arXiv.1012.2599.

[96] A. Hjorth Larsen et al., "The atomic simulation environment—a python library for working with atoms", *Journal of Physics: Condensed Matter*, vol. 29, no. 27, pp. 1–31, 2017. DOI: 10.1088/1361-648X/aa680e.

[97] V. Blum et al., "Ab initio molecular simulations with numeric atom-centered orbitals", *Computer Physics Communications*, vol. 180, no. 11, pp. 2175–2196, 2009. DOI: 10.1016/j.cpc.2009.06.022.

[98] H. Kim and G. Kim, "Adsorption properties of dopamine derivatives using carbon nanotubes: A first-principles study", *Applied Surface Science*, vol. 501, p. 144 249, 2020. DOI: 10.1016/j.apsusc.2019.144249.

[99] N. Srinivas, A. Krause, S. M. Kakade, and M. Seeger, "Gaussian Process Optimization in the Bandit Setting: No Regret and Experimental Design", *IEEE Transactions on Information Theory*, vol. 58, no. 5, pp. 3250–3265, 2012. DOI: 10.1109/TIT.2011.2182033.

[100] R. H. Byrd, P. Lu, J. Nocedal, and C. Zhu, "A Limited Memory Algorithm for Bound Constrained Optimization", *SIAM Journal on Scientific Computing*, vol. 16, no. 5, pp. 1190–1208, 1995. DOI: 10.1137/0916069.

[101] A. Calvi, A. Ferrari, L. Sbuelz, A. Goldoni, and S. Modesti, "Recognizing Physisorption and Chemisorption in Carbon Nanotubes Gas Sensors by Double Exponential Fitting of the Response", *Sensors*, no. 5, p. 731, 2016. DOI: 10.3390/s16050731.

[102] United Nations, *The 17 goals | sustainable development*. Accessed: Jan. 12, 2026. [Online]. Available: https://sdgs.un.org/goals.

[103] United Nations, "The sustainable development goals report 2025", United Nations, 2025. Accessed: Jan. 12, 2026. [Online]. Available: https://unstats.un.org/sdgs/files/report/2025/secretary-general-sdg-report-2025--EN.pdf.

[104] United Nations Children's Fund (UNICEF), "Triple threat: The impact of water, sanitation and hygiene on child health", United Nations Children's Fund (UNICEF), 2023. Accessed: Jan. 12, 2026. [Online]. Available: https://www.unicef.org/media/137206/file/triple-threat-wash-EN.pdf.

[105] United Nations Educational, Scientific and Cultural Organization (UNESCO), *Statistics from the un world water development report*, 2024. Accessed: Nov. 30, 2025. [Online]. Available: https://www.unesco.org/reports/wwdr/en/2024/s.

[106] R. Bain, R. Johnston, S. Khan, A. Hancioglu, and T. Slaymaker, "Monitoring Drinking Water Quality in Nationally Representative Household Surveys in Low- and Middle-Income Countries: Cross-Sectional Analysis of 27 Multiple Indicator Cluster Surveys 2014–2020", *Environmental Health Perspectives*, vol. 129, no. 9, p. 097 010, 2021. DOI: 10.1289/EHP8459.

[107] G. M. Kremer, "The boltzmann equation", in *An Introduction to the Boltzmann Equation and Transport Processes in Gases*. Berlin, Heidelberg: Springer Berlin Heidelberg, 2010, pp. 37–80. DOI: 10.1007/978-3-642-11696-4_2.